

Analysis of the central-moments-based lattice Boltzmann method for the numerical modelling of the one-dimensional advection-diffusion equation: Equivalent finite difference and partial differential equations

Goncalo Silva

IDMEC, Escola de Ciências e Tecnologia, Universidade de Évora, R. Romão Ramalho 59, 7000-671 Évora, Portugal

ARTICLE INFO

MSC:
00-01
99-00

Keywords:

Lattice Boltzmann method
Central moments collision scheme
Advection-diffusion equations
Truncation error analysis
Stability analysis

ABSTRACT

This work presents a detailed theoretical analysis of the multiple-relaxation-time (MRT) lattice Boltzmann method (LBM), formulated on central moment (CM) space, for the numerical modelling of the one-dimensional advection-diffusion equation (ADE) with a constant velocity and diffusion coefficient, based on the D1Q3 lattice. Other LBM collision operators, such as single-relaxation-time Bhatnagar–Gross–Krook (BGK), regularized (REG) and MRT in raw moment (RM) space are also considered in this study. Without recurring to asymptotic analyses, such as the Chapman–Enskog expansion, we investigate the approximation of the MRT-CM with respect to the ADE by deriving its equivalent finite difference (EFD) scheme, which obeys an explicit four-level finite difference scheme at discrete level. Its steady-state limit follows a standard central differencing scheme for the steady ADE, yet with possible artefacts in the effective diffusion coefficient. Then, through the Taylor expansion of the EFD scheme, a detailed accuracy analysis, based on the equivalent partial differential (EPD) equation, reveals the leading order truncation errors associated with each collision model under study. Although MRT-CM and MRT-RM models have similar error structures, the former has a much reduced and simpler form, particularly in the dispersion error term, which might explain the improved Galilean invariance of the CM model. Through a suitable combination of the MRT free parameters (either in RM or CM bases), it is possible to improve its accuracy from second- to fourth-order. After that, we study the necessary and sufficient stability conditions of the MRT-CM, and its relation with other collision operators, based on the von Neumann stability analysis of the derived EFD schemes. Unexpectedly, the MRT-CM appears to support a narrower stability domain than the MRT-RM model, particularly at higher advection velocities, which can be tracked down to the inclusion of additional terms in the stability condition of the former that scale with higher order polynomials of the advection velocity. Finally, some numerical tests for the ADE on 1D unbounded domains are conducted, which confirm this work theoretical conclusions on the MRT-CM performance.

1. Introduction

In the last decades, the lattice Boltzmann method (LBM) [1–4] has gained wide popularity among Fluid Mechanics community as an alternative technique within Computational Fluid Dynamics (CFD) field [5,6]. The method attractiveness is mainly credited to its ability to solve complex physical problems through a simple and efficient algorithm [1–4]. In a nutshell, the LBM solves the fluid flow equations and/or related conservation laws at macroscopic level through a simplified kinetic model where the time–space evolution of idealized entities, so-called LBM populations, is described through a succession of streaming and collision steps. While the streaming step is standard and executes a simple shift of these populations, the collision step has a much richer content, being responsible for the physics to be modelled. Consequently, many different approaches to realize the LBM collision process have been proposed [7]. Popular LBM collision models span from the simplest single-relaxation-time Bhatnagar–Gross–Krook (BGK) [8] to the most general multiple-relaxation-time (MRT) [9,10]. Despite differences in structure, these models have in common the adoption of a static frame to realize the collisions. Adopting a distinct viewpoint, Geier [11] proposed the realization of collisions in a comoving reference frame. The resulting model was originally coined as the cascaded LBM [11] to express its hierarchical way of dealing with moments in the collision algorithm, in which higher-order moments are constructed from lower-order ones in a cascade-like fashion. Further developments on the idea led to a more general formulation where collisions are performed in the central moment space [7,12–16], popularizing the name “central moment” LBM

E-mail address: gnsilva@uevora.pt.

<https://doi.org/10.1016/j.compfluid.2024.106535>

Received 22 October 2024; Received in revised form 12 December 2024; Accepted 20 December 2024

Available online 2 January 2025

0045-7930/© 2025 The Author. Published by Elsevier Ltd. This is an open access article under the CC BY license (<http://creativecommons.org/licenses/by/4.0/>).

(CM-LBM). This terminology reflects the distinctive operation principle of the CM-LBM in that moments are shifted by the macroscopic velocity, in contrast to the raw moments approach where collisions take place in a frame at rest [7]. In fact, the premise behind the CM-LBM formulation has a sound physical basis as it roots on the principle of frame-indifference. Transcribing from Woods [17] “*frame-indifference is the essential property distinguishing diffusion from convection*”. Putting this statement into LBM context, and bearing in mind that the relaxation of moments is what determines the rate of diffusion phenomena at macroscopic level, then satisfaction with the frame-indifference principle seems to imply that the collision step should be performed on a comoving frame in order to avoid the interference of convection over diffusion. Such an idea quickly gained traction among LBM community, resulting in a series of works adopting the CM-LBM in the modelling of hydrodynamics [11,14,18–22] and scalar transport [21–26] problems.

In retrospect, soon after Geier’s original proposition of the CM-LBM [11], the same author refined his first work to improve the model Galilean-invariance [27]. About the same time period, Asinari [28] showed how the cascaded model algorithm could be retrieved from the MRT static scheme subject to shift matrices. Lycett-Brown [19] proposed a simplified derivation of the cascaded algorithm [11], and Dubois and Février [12,13] reformulated the cascaded model to operate on the central moment space. Following these efforts, De Rosis [29,30] proposed further modifications to the original cascaded scheme, such as the adoption of a nonorthogonal basis instead of the orthogonal basis of central moments and the relaxation of moments towards discrete second-order truncated equilibrium populations instead of the equilibrium state of the continuous Maxwellian distribution. In a very thorough and systematic assessment on the role of collision models in LBM, Coreixas et al. [7] presented a pure theoretical analysis of the CM-LBM scheme, identifying differences and similarities between dynamic and static frame collision models, considering several moment space bases. Compared to the standard raw moment space formulation, the work [7] indicated that CM-LBM introduced the following two main modifications: (i) the collision is operated on the central moment space and (ii) the equilibrium state used in the relaxation process is expanded up to higher-order terms [16], which exceeds the second order truncation typically adopted in the equilibrium [8,31]. According to [7], it is the extended equilibrium used by the CM-LBM, rather than the central moment space formulation, the main cause for the observed stability enhancements; a result that appears common to other collision models as, in an earlier work [32], the use of an extended equilibrium was also shown to enhance the numerical stability of the LBM formulated in the raw moment (RM) space. Based on an extensive linear stability analysis, Wissocq and Sagaut [33] investigated the impact of the numerical hyperviscosity on different LBM collision models and confirmed the key role played by extended equilibrium formulation on the CM-LBM stability characteristics. However, perhaps with the exception of Dubois and Février works [12,13], a study dedicated to investigate the isolated impact of the central moment formulation on the model stability, putting aside the role of the extended equilibrium, is still lacking. At the same time, the impact of the CM-LBM formulation on the model accuracy is also a subject under scrutiny. While the CM-LBM is often credited to be a more accurate model (a claim typically supported on numerical outcomes [11,29,30]), more rigorous and insightful theoretical analyses to justify the observed accuracy gains remain scarce. In this context, it is worth highlighting the exceptions due to Geier [27] and Dubois and Février [12], which performed a third-order asymptotic analyses on the CM-LBM in order to disclose the structure of the leading-order dispersion terms, and also the work by Wissocq and Sagaut [33] that presented an extended asymptotic analyses of the CM-LBM, up to the fourth order, to investigate the hyperviscosity corrections on the model dissipation. Finally, it is important to refer the work by Straka and Sharma [25], which thoroughly derived the exact equivalent finite difference and the fourth order modified partial differential equations of the CM-LBM for the advection-diffusion equation in a 1D setting with the purpose of assessing its accuracy and stability characteristics. Unfortunately, the work [25] considered a single-relaxation-time formulation of the CM-LBM which, as will be shown in the present work, makes the CM-LBM model to effectively reduce to the standard BGK [8] in a static reference frame. Therefore, the present work intends to redo the analyses of [25], but in a MRT framework, so that the unique traits of the CM-LBM formulation can *de facto* be assessed.

With this contribution, one intends to study the stability and accuracy characteristics of the CM-LBM by rewriting it as an equivalent finite difference (EFD) scheme, which will then allow us to use the common tools of numerical analysis, such as the linear von Neumann stability analysis or the modified partial differential equations approach [5,34–36]. This methodology contrasts with the standard theoretical approaches followed in LBM, where the relation between the LBM mesoscopic equations with respect to the intended macroscopic partial differential equations is commonly established through asymptotic analyses such as the Chapman–Enskog expansion [1,17,37], the asymptotic expansion with diffusive scaling [38], the Maxwell iteration [39,40], the direct Taylor expansion [41–43], or the recurrence equation [44,45] methodologies. Despite their algorithmic differences, these asymptotic analysis methods end up producing identical macroscopic equations, at least, up to second-order, as shown by Chai and Shi [46]. However, they also have in common the fact that their extensions to higher orders, i.e. beyond the second order, are considerably more hard-working, typically evolving lengthy algebraic manipulations, which explains why so few works based on higher order asymptotic analyses have been performed [45]. Nonetheless, to reach out a more complete picture of the LBM scheme, the assessment of those higher order terms [12,27,33,41,45,47] is fundamental (e.g., to assess the leading truncation errors in the numerical approximation) or, in the limit, it is even necessary to have the full knowledge of the LBM scheme at discrete level [48–52] (e.g., to construct adequate discretization strategies for well-balanced LBM schemes).

To gain a deeper insight into the error structure of the LBM, many efforts have been devoted to rewriting LBM as a EFD scheme [44,53–57]. However, until recently, those attempts have relied upon laborious and ingenious mathematical manipulations of the LBM equations, which could only be worked out under particular and simplified cases [48–52,58]. To circumvent those limitations, Fůcık and Straka [59] and Bellotti et al. [60], in an independent manner, recently proposed two general methods to derive the EFD scheme of any LBM, with the work [59] following a more algorithmic-based approach while the work [60] pursuing a more mathematical oriented framework. For its simplicity, transparency and mathematical rigour, Bellotti’s approach [60] will be adopted in this work; a choice also preferred by others [61–63]. Based on [60], one will derive the EFD scheme of the CM-LBM approximation of the 1D time-dependent ADE. This framework is typically employed in the modelling of transport phenomena, finding application in many practical instances [64]. However, for our theoretical interest, we will consider the ADE model essentially for the reason it is the simplest physical setting where both fluid advection and diffusion coexist. In this way, it will be possible to assess in a rigorous theoretical manner how the comoving frame formulation of the CM-LBM exactly handles these two phenomena and whether the comoving frame modelling actually meets the promised benefits in terms of stability and accuracy compared to the static frame formulation adopted by the LBM in the RM space [65,66]. In that sense, the present work can be considered as an extension of the analysis recently presented by Chen et al. [61] for the RM-LBM towards the CM-LBM scheme. We note that Fůcık and Straka [59] have already presented the equivalent finite difference and partial differential equations of the CM-LBM for this problem class in one of the appendices of their work, yet no discussion has been given to the numerical characteristics of the scheme. To fill that gap, this work will rederive [59], based on the systematic methodology of [60], and then provide a critical analysis on: (i) its discrete structure, (ii) the form of the leading order truncation errors, and (iii) the exact stability properties of the CM-LBM scheme.

The remainder of the manuscript is organized as follows. Section 2 introduces the 1D time-dependent ADE and its CM-LBM modelling. Section 3 derives the EFD scheme of the CM-LBM by employing, for the first time, the methodology of [60] for the LBM in the CM space, followed by a critical analysis on the differences between the resting and comoving reference frames. Then, Section 4 extends this study over the steady-state ADE. Section 5 performs an accuracy analysis by inspecting the leading order truncation errors of the different LBM collision models considered herein. Section 6 develops an exact von Neumann linear stability analysis of the CM-LBM scheme, checking the differences and similarities with respect to the RM-LBM formulation. Section 7 displays some numerical experiments to confirm the theoretical analyses performed throughout this work. Finally, Section 8 concludes the work with a summary of the main findings.

2. Lattice Boltzmann method for advection diffusion equation

2.1. Advection diffusion equation in 1D

Consider the 1D time-dependent advection diffusion equation (ADE), which governs the transport of the unknown scalar quantity ϕ that is simultaneously carried by a uniform velocity field u with a constant diffusion coefficient D . Such a 1D time-dependent ADE is a textbook problem [64] described by the following partial differential equation:

$$\frac{\partial \phi}{\partial t} + u \frac{\partial \phi}{\partial x} = D \frac{\partial^2 \phi}{\partial x^2}. \quad (1)$$

Eq. (1) is the simplest physical setting where both fluid advection and diffusion play an important role. Therefore, we will consider it as a test model to evaluate whether the central moment (CM) space formulation of lattice Boltzmann method (LBM) will bring any improvements for accuracy and stability.

2.2. Lattice Boltzmann method in central moment space

The LBM solves for the populations $f_i(\mathbf{x}, t)$, defined on space \mathbf{x} and time t , along a discrete velocity set, called lattice, featuring one immobile $c_0 = \mathbf{0}$ and $q - 1$ non-zero velocity vectors c_i per grid node. The populations $f_i(\mathbf{x}, t)$ evolve throughout space and time along a succession of stream-and-collide steps. For generality, the multiple-relaxation-time (MRT) collision model is considered in this work. On this basis, the traditional stream-and-collide algorithm of the LBM-MRT equation is written as a two step process as follows:

$$f_i(\mathbf{x} + c_i \Delta t, t + \Delta t) = \hat{f}_i(\mathbf{x}, t), \quad (2a)$$

$$\hat{f}_i(\mathbf{x}, t) = f_i(\mathbf{x}, t) - (\mathbf{M}^{-1} \mathbf{S} \mathbf{M})_{ik} [f_k(\mathbf{x}, t) - f_k^{\text{eq}}(\mathbf{x}, t)]. \quad (2b)$$

where \mathbf{M} is a transformation matrix and \mathbf{S} is a diagonal relaxation matrix. This work considers the D1Q3 lattice model with the discrete velocity set:

$$\mathbf{c}_i = \begin{cases} -c, & i = -1, \\ 0, & i = 0, \\ c, & i = 1, \end{cases} \quad (3)$$

where $c = \Delta x / \Delta t$ is the lattice speed with Δx the lattice spacing and Δt the time step. In central moment (CM) space the transformation \mathbf{M} and relaxation \mathbf{S} matrices are given by [7,12,13,25,33]:

$$\mathbf{M} = \begin{pmatrix} 1 & 1 & 1 \\ -u & (c-u) & (-c-u) \\ u^2 & (c-u)^2 & (-c-u)^2 \end{pmatrix}, \quad \mathbf{S} = \begin{pmatrix} s_0 & 0 & 0 \\ 0 & s_1 & 0 \\ 0 & 0 & s_2 \end{pmatrix}, \quad \mathbf{M}^{-1} = \begin{pmatrix} \frac{(c-u)(c+u)}{c^2} & -\frac{2u}{c^2} & -\frac{1}{c^2} \\ \frac{u(c+u)}{2c^2} & \frac{c+2u}{2c^2} & \frac{1}{2c^2} \\ -\frac{u(c-u)}{2} & -\frac{c-2u}{2c} & \frac{1}{2c^2} \end{pmatrix}, \quad (4)$$

where a comoving reference frame with respect to the uniform macroscopic fluid velocity u is considered. The relaxation rates s_i in matrix \mathbf{S} are bounded to the (0, 2) interval to guarantee the positivity of the modelled macroscopic transport coefficient D in the LBM approximation of Eq. (1). Note that, when $\mathbf{M}(u = 0)$ in Eq. (4), the standard MRT transformation matrix on a raw moment (RM) space is recovered [3,10,61].

To approximate the macroscopic ADE, Eq. (1), the LBM equilibrium presented in [61] is considered:

$$f_i^{\text{eq}} = \omega_i \phi \left[1 + \frac{c_i u}{c_s^2} + \eta \frac{u^2 (c_i^2 - c_s^2)}{2c_s^4} \right], \quad (5)$$

where

$$c_s^2 = (1 - \omega_0) c^2, \quad (6a)$$

$$\eta = \frac{2(1 - \omega_0)}{\omega_0}, \quad (6b)$$

$$\omega_1 = \omega_{-1} = \frac{1 - \omega_0}{2}, \quad (6c)$$

and $0 < \omega_0 < 1$ to ensure that all weight coefficients are larger than zero.

In the D1Q3 model, the equilibrium, given by Eq. (5) with Eq. (6), is expressed in populations space as follows:

$$\begin{bmatrix} f_0^{\text{eq}} \\ f_1^{\text{eq}} \\ f_{-1}^{\text{eq}} \end{bmatrix} = \begin{bmatrix} \omega_0 \phi - \frac{u^2}{c^2} \phi \\ \frac{(1-\omega_0)}{2} \phi + \frac{u}{2c} \phi + \frac{u^2}{2c^2} \phi \\ \frac{(1-\omega_0)}{2} \phi - \frac{u}{2c} \phi + \frac{u^2}{2c^2} \phi \end{bmatrix}. \quad (7)$$

The equilibrium moments $\mathbf{m} = \mathbf{M} \mathbf{f}^{\text{eq}}$ mapped onto raw moment (RM) space, i.e. $\mathbf{M}(u=0)$ in Eq. (4), read:

$$\begin{bmatrix} m_0^{\text{eq}} \\ m_1^{\text{eq}} \\ m_{-1}^{\text{eq}} \end{bmatrix} = \begin{bmatrix} \phi \\ u\phi \\ \underbrace{(1-w_0)c^2+u^2}_{=c_s^2} \phi \end{bmatrix}, \quad (8)$$

and mapped onto central moment (CM) space using \mathbf{M} in Eq. (4) read:

$$\begin{bmatrix} m_0^{\text{eq}} \\ m_1^{\text{eq}} \\ m_{-1}^{\text{eq}} \end{bmatrix} = \begin{bmatrix} \phi \\ 0 \\ \underbrace{(1-w_0)c^2}_{=c_s^2} \phi \end{bmatrix}. \quad (9)$$

3. Equivalent Finite Difference (EFD) scheme of the CM-LBM

This section reviews the procedure, originally proposed by Bellotti et al. [60], to obtain the equivalent finite difference (EFD) scheme of the LBM [Eq. (2)] for the solution of the ADE [Eq. (1)]; more details can be found in [60,61].

First, let us explicitly write the collision step, Eq. (2b), in moment space, $\hat{\mathbf{m}} = \mathbf{M} \hat{\mathbf{f}}$, as follows:

$$\hat{\mathbf{m}}(\mathbf{x}, t) = (\mathbf{I} - \mathbf{S}) \mathbf{m}(\mathbf{x}, t) + \mathbf{S} \mathbf{m}^{\text{eq}}(\mathbf{x}, t). \quad (10)$$

Second, let us repeat this task for the streaming step, Eq. (2a). To this end, it is convenient to introduce the shift operator $T_{\Delta x}^{c_k/c}$ defined as $T_{\Delta x}^{c_k/c} [f_i(\mathbf{x}, t)] = f_i(\mathbf{x} - c_k \Delta t, t)$, which allows us to write the streaming effect over populations as a shift matrix [60,61]. Based on this formalism, the streaming step in the D1Q3 model can be explicitly written as:

$$f_i(\mathbf{x} + c_i \Delta t, t + \Delta t) = \text{diag} \left(T_{\Delta x}^{c_0/c}, T_{\Delta x}^{c_1/c}, T_{\Delta x}^{c_{-1}/c} \right) \hat{f}_i(\mathbf{x} + c_i \Delta t, t), \quad (11)$$

where $f_i = (f_0, f_1, f_{-1})^T$ and $c_i = (c_0, c_1, c_{-1})^T$. Then, let us shift the analysis from $\mathbf{x} + c_i \Delta t$ to the \mathbf{x} location and multiply both sides of Eq. (11) by \mathbf{M}_{ik} so that:

$$\underbrace{\mathbf{M}_{ik} f_i(\mathbf{x}, t + \Delta t)}_{=\mathbf{m}^{n+1}} = \underbrace{\left(\mathbf{M} \text{diag} \left(T_{\Delta x}^{c_0/c}, T_{\Delta x}^{c_1/c}, T_{\Delta x}^{c_{-1}/c} \right) \mathbf{M}^{-1} \right)}_{=\mathbf{T}} \underbrace{\mathbf{M}_{ik} \hat{f}_i(\mathbf{x}, t)}_{=\hat{\mathbf{m}}^n}. \quad (12)$$

Now, introduce Eq. (10) into Eq. (12). To alleviate the notation, we will drop the (\mathbf{x}, t) dependency on Eq. (10) and rewrite it as follows $\hat{\mathbf{m}}^n(\mathbf{x}) = (\mathbf{I} - \mathbf{S}) \mathbf{m}^n(\mathbf{x}) + \mathbf{S} \mathbf{m}^{\text{eq}n}(\mathbf{x})$. According to this notation, Eq. (12) can be written as $\mathbf{m}^{n+1} = \mathbf{T} \hat{\mathbf{m}}^n$. Combining these two equations we can rewrite the stream-and-collide algorithm of the LBM on moment space as follows:

$$\mathbf{m}^{n+1}(\mathbf{x}) = \mathbf{P} \mathbf{m}^n(\mathbf{x}) + \mathbf{Q} \mathbf{m}^{\text{eq}n}(\mathbf{x}). \quad (13)$$

where $\mathbf{m}^n(\mathbf{x}) = \mathbf{m}(\mathbf{x}, t_n)$, $\mathbf{T} := \mathbf{M} \text{diag} \left(T_{\Delta x}^{c_0/c}, T_{\Delta x}^{c_1/c}, T_{\Delta x}^{c_{-1}/c} \right) \mathbf{M}^{-1}$, $\mathbf{P} := \mathbf{T} (\mathbf{I} - \mathbf{S})$, and $\mathbf{Q} := \mathbf{T} \mathbf{S}$.

Next, we apply Eq. (13) in itself recursively k time steps, up to filling in the q steps. In the end, we recover:

$$\mathbf{m}^{n+1}(\mathbf{x}) = \mathbf{P}^k \mathbf{m}^{n-k+1}(\mathbf{x}) + \sum_{l=0}^{k-1} \mathbf{P}^l \mathbf{Q} \mathbf{m}^{\text{eq}n-l}(\mathbf{x}), \quad \forall k \in \mathbb{N}. \quad (14)$$

At this point, it is useful to consider the change of variables $\bar{n} + k = n + 1$ into Eq. (14), which leads to:

$$\mathbf{m}^{\bar{n}+k}(\mathbf{x}) = \mathbf{P}^k \mathbf{m}^{\bar{n}}(\mathbf{x}) + \sum_{l=0}^{k-1} \mathbf{P}^l \mathbf{Q} \mathbf{m}^{\text{eq}|\bar{n}+k-1-l}(\mathbf{x}) \quad (15)$$

Now, let us apply to each side of Eq. (15) the sum $\sum_{k=0}^q \gamma_k$, where γ_k are the coefficients of the characteristic polynomial $\chi_P = \sum_{k=0}^q \gamma_k \mathbf{X}^k$ of the matrix \mathbf{P} . Then, by invoking the Cayley–Hamilton theorem [60], expressed by $\sum_{k=0}^q \gamma_k \mathbf{P}^k = \mathbf{0}$, it is possible to rewrite Eq. (15) as follows:

$$\sum_{k=0}^q \gamma_k \mathbf{m}^{\bar{n}+k}(\mathbf{x}) = \underbrace{\left(\sum_{k=0}^q \gamma_k \mathbf{P}^k \right)}_{=0} \mathbf{m}^{\bar{n}}(\mathbf{x}) + \sum_{k=0}^q \gamma_k \left(\sum_{l=0}^{k-1} \mathbf{P}^l \mathbf{Q} \mathbf{m}^{\text{eq}|\bar{n}+k-1-l}(\mathbf{x}) \right). \quad (16)$$

Developing the term on the left-hand-side and re-introducing the change of variables $\bar{n} + q = n + 1$ in Eq. (16) we obtain:

$$\mathbf{m}^{n+1}(\mathbf{x}) = - \sum_{k=0}^{q-1} \gamma_k \mathbf{m}^{n+1-q+k}(\mathbf{x}) + \sum_{k=0}^q \gamma_k \left(\sum_{l=0}^{k-1} \mathbf{P}^l \mathbf{Q} \mathbf{m}^{\text{eq}n-q+k-l}(\mathbf{x}) \right). \quad (17)$$

Eq. (17) can be further simplified by recognizing that the last sum may start from $k = 1$ and in the last double sum the indices can be interchanged so that it can be explicitly rewritten as follows:

$$\mathbf{m}^{n+1}(\mathbf{x}) = - \sum_{k=0}^{q-1} \gamma_k \mathbf{m}^{n+1-q+k}(\mathbf{x}) + \sum_{k=0}^{q-1} \left(\sum_{l=0}^k \gamma_{q+l-k} \mathbf{P}^l \right) \mathbf{Q} \mathbf{m}^{\text{eq}n-k}(\mathbf{x}). \quad (18)$$

Referring to the particular case of the D1Q3 model, $q = 3$, and focusing on the evolution of the conserved moment $m_0^n(x_j) = \phi_j^n := \phi(j\Delta x, t_n)$, then Eq. (18) leads to the equivalent finite difference (EFD) scheme representation of the LBM modelling of the 1D time-dependent ADE:

$$\phi_j^{n+1} = - \sum_{k=0}^2 \gamma_k \phi_j^{n+k-2} + \left[\sum_{k=0}^2 \left(\sum_{l=0}^k \gamma_{l-k+3} P^l \right) Q m_j^{\text{eq}|n-k} \right]_0. \quad (19)$$

Up to this point, the derivation leading up to Eq. (19) was developed without details regarding the LBM collision operator. Now, let us consider the collision in the central moment space [Eq. (4)] so that matrices T , P and Q are expressed as:

$$\begin{aligned} T &= \mathbf{M} \text{diag} \left(T_{\Delta x}^{c_0/c}, T_{\Delta x}^{c_1/c}, T_{\Delta x}^{c_{-1}/c} \right) \mathbf{M}^{-1} \\ &= \begin{pmatrix} \frac{1}{2} \left(2T_{\Delta x}^{c_0/c} + \frac{u}{c} \left(T_{\Delta x}^{c_1/c} - T_{\Delta x}^{c_{-1}/c} \right) + \frac{u^2}{c^2} \left(T_{\Delta x}^{c_1/c} - 2T_{\Delta x}^{c_0/c} + T_{\Delta x}^{c_{-1}/c} \right) \right) & & \\ \frac{c}{2} \left(\frac{u}{c} \left(T_{\Delta x}^{c_1/c} - 2T_{\Delta x}^{c_0/c} + T_{\Delta x}^{c_{-1}/c} \right) - \frac{u^2}{c^2} \left(T_{\Delta x}^{c_1/c} - 2T_{\Delta x}^{c_0/c} + T_{\Delta x}^{c_{-1}/c} \right) \right) & \dots & \\ \frac{c^2}{2} \left(\frac{u}{c} \left(T_{\Delta x}^{c_1/c} - T_{\Delta x}^{c_{-1}/c} \right) - \frac{u^2}{c^2} \left(T_{\Delta x}^{c_1/c} - 2T_{\Delta x}^{c_0/c} + T_{\Delta x}^{c_{-1}/c} \right) - \frac{u^3}{c^3} \left(T_{\Delta x}^{c_1/c} - T_{\Delta x}^{c_{-1}/c} \right) + \frac{u^4}{c^4} \left(T_{\Delta x}^{c_1/c} - 2T_{\Delta x}^{c_0/c} + T_{\Delta x}^{c_{-1}/c} \right) \right) & & \\ \frac{1}{2c} \left(\left(T_{\Delta x}^{c_1/c} - T_{\Delta x}^{c_{-1}/c} \right) + \frac{u}{c} \left(2T_{\Delta x}^{c_1/c} - 4T_{\Delta x}^{c_0/c} + 2T_{\Delta x}^{c_{-1}/c} \right) \right) & & \\ \dots & \frac{1}{2} \left(\left(T_{\Delta x}^{c_1/c} + T_{\Delta x}^{c_{-1}/c} \right) + \frac{u}{c} \left(T_{\Delta x}^{c_1/c} - T_{\Delta x}^{c_{-1}/c} \right) - \frac{u^2}{c^2} \left(2T_{\Delta x}^{c_1/c} - 4T_{\Delta x}^{c_0/c} + 2T_{\Delta x}^{c_{-1}/c} \right) \right) & \dots \\ \frac{c}{2} \left(\left(T_{\Delta x}^{c_1/c} - T_{\Delta x}^{c_{-1}/c} \right) - \frac{u^2}{c^2} \left(3T_{\Delta x}^{c_1/c} - 3T_{\Delta x}^{c_{-1}/c} \right) + \frac{u^3}{c^3} \left(2T_{\Delta x}^{c_1/c} - 4T_{\Delta x}^{c_0/c} + 2T_{\Delta x}^{c_{-1}/c} \right) \right) & & \\ \dots & \frac{1}{2c^2} \left(T_{\Delta x}^{c_1/c} - 2T_{\Delta x}^{c_0/c} + T_{\Delta x}^{c_{-1}/c} \right) & \\ \dots & \frac{1}{2c} \left(\left(T_{\Delta x}^{c_1/c} - T_{\Delta x}^{c_{-1}/c} \right) - \frac{u}{c} \left(T_{\Delta x}^{c_1/c} - 2T_{\Delta x}^{c_0/c} + T_{\Delta x}^{c_{-1}/c} \right) \right) & \\ \frac{1}{2} \left(\left(T_{\Delta x}^{c_1/c} + T_{\Delta x}^{c_{-1}/c} \right) - \frac{u}{c} \left(T_{\Delta x}^{c_1/c} - T_{\Delta x}^{c_{-1}/c} \right) + \frac{u^2}{c^2} \left(T_{\Delta x}^{c_1/c} - 2T_{\Delta x}^{c_0/c} + T_{\Delta x}^{c_{-1}/c} \right) \right) & & \end{pmatrix}, \quad (20) \end{aligned}$$

$$\begin{aligned} P &= T(I - S) \\ &= \begin{pmatrix} \frac{(1-s_0)}{2} \left(2T_{\Delta x}^{c_0/c} + \frac{u}{c} \left(T_{\Delta x}^{c_1/c} - T_{\Delta x}^{c_{-1}/c} \right) + \frac{u^2}{c^2} \left(T_{\Delta x}^{c_1/c} - 2T_{\Delta x}^{c_0/c} + T_{\Delta x}^{c_{-1}/c} \right) \right) & & \\ \frac{c(1-s_0)}{2} \left(\frac{u}{c} \left(T_{\Delta x}^{c_1/c} - 2T_{\Delta x}^{c_0/c} + T_{\Delta x}^{c_{-1}/c} \right) - \frac{u^2}{c^2} \left(T_{\Delta x}^{c_1/c} - 2T_{\Delta x}^{c_0/c} + T_{\Delta x}^{c_{-1}/c} \right) \right) & \dots & \\ \frac{c^2(1-s_0)}{2} \left(\frac{u}{c} \left(T_{\Delta x}^{c_1/c} - T_{\Delta x}^{c_{-1}/c} \right) - \frac{u^2}{c^2} \left(T_{\Delta x}^{c_1/c} - 2T_{\Delta x}^{c_0/c} + T_{\Delta x}^{c_{-1}/c} \right) - \frac{u^3}{c^3} \left(T_{\Delta x}^{c_1/c} - T_{\Delta x}^{c_{-1}/c} \right) + \frac{u^4}{c^4} \left(T_{\Delta x}^{c_1/c} - 2T_{\Delta x}^{c_0/c} + T_{\Delta x}^{c_{-1}/c} \right) \right) & & \\ \frac{(1-s_1)}{2c} \left(\left(T_{\Delta x}^{c_1/c} - T_{\Delta x}^{c_{-1}/c} \right) + \frac{u}{c} \left(2T_{\Delta x}^{c_1/c} - 4T_{\Delta x}^{c_0/c} + 2T_{\Delta x}^{c_{-1}/c} \right) \right) & & \\ \dots & \frac{(1-s_1)}{2} \left(\left(T_{\Delta x}^{c_1/c} + T_{\Delta x}^{c_{-1}/c} \right) + \frac{u}{c} \left(T_{\Delta x}^{c_1/c} - T_{\Delta x}^{c_{-1}/c} \right) - \frac{u^2}{c^2} \left(2T_{\Delta x}^{c_1/c} - 4T_{\Delta x}^{c_0/c} + 2T_{\Delta x}^{c_{-1}/c} \right) \right) & \dots \\ \frac{c(1-s_1)}{2} \left(\left(T_{\Delta x}^{c_1/c} - T_{\Delta x}^{c_{-1}/c} \right) - \frac{u^2}{c^2} \left(3T_{\Delta x}^{c_1/c} - 3T_{\Delta x}^{c_{-1}/c} \right) + \frac{u^3}{c^3} \left(2T_{\Delta x}^{c_1/c} - 4T_{\Delta x}^{c_0/c} + 2T_{\Delta x}^{c_{-1}/c} \right) \right) & & \\ \dots & \frac{(1-s_2)}{2c^2} \left(T_{\Delta x}^{c_1/c} - 2T_{\Delta x}^{c_0/c} + T_{\Delta x}^{c_{-1}/c} \right) & \\ \dots & \frac{(1-s_2)}{2c} \left(\left(T_{\Delta x}^{c_1/c} - T_{\Delta x}^{c_{-1}/c} \right) - \frac{u}{c} \left(T_{\Delta x}^{c_1/c} - 2T_{\Delta x}^{c_0/c} + T_{\Delta x}^{c_{-1}/c} \right) \right) & \\ \frac{(1-s_2)}{2} \left(\left(T_{\Delta x}^{c_1/c} + T_{\Delta x}^{c_{-1}/c} \right) - \frac{u}{c} \left(T_{\Delta x}^{c_1/c} - T_{\Delta x}^{c_{-1}/c} \right) + \frac{u^2}{c^2} \left(T_{\Delta x}^{c_1/c} - 2T_{\Delta x}^{c_0/c} + T_{\Delta x}^{c_{-1}/c} \right) \right) & & \end{pmatrix}, \quad (21) \end{aligned}$$

$$\begin{aligned} Q &= T S \\ &= \begin{pmatrix} \frac{s_0}{2} \left(2T_{\Delta x}^{c_0/c} + \frac{u}{c} \left(T_{\Delta x}^{c_1/c} - T_{\Delta x}^{c_{-1}/c} \right) + \frac{u^2}{c^2} \left(T_{\Delta x}^{c_1/c} - 2T_{\Delta x}^{c_0/c} + T_{\Delta x}^{c_{-1}/c} \right) \right) & & \\ \frac{c s_0}{2} \left(\frac{u}{c} \left(T_{\Delta x}^{c_1/c} - 2T_{\Delta x}^{c_0/c} + T_{\Delta x}^{c_{-1}/c} \right) - \frac{u^2}{c^2} \left(T_{\Delta x}^{c_1/c} - 2T_{\Delta x}^{c_0/c} + T_{\Delta x}^{c_{-1}/c} \right) \right) & \dots & \\ \frac{c^2 s_0}{2} \left(\frac{u}{c} \left(T_{\Delta x}^{c_1/c} - T_{\Delta x}^{c_{-1}/c} \right) - \frac{u^2}{c^2} \left(T_{\Delta x}^{c_1/c} - 2T_{\Delta x}^{c_0/c} + T_{\Delta x}^{c_{-1}/c} \right) - \frac{u^3}{c^3} \left(T_{\Delta x}^{c_1/c} - T_{\Delta x}^{c_{-1}/c} \right) + \frac{u^4}{c^4} \left(T_{\Delta x}^{c_1/c} - 2T_{\Delta x}^{c_0/c} + T_{\Delta x}^{c_{-1}/c} \right) \right) & & \\ \frac{s_1}{2c} \left(\left(T_{\Delta x}^{c_1/c} - T_{\Delta x}^{c_{-1}/c} \right) + \frac{u}{c} \left(2T_{\Delta x}^{c_1/c} - 4T_{\Delta x}^{c_0/c} + 2T_{\Delta x}^{c_{-1}/c} \right) \right) & & \\ \dots & \frac{s_1}{2} \left(\left(T_{\Delta x}^{c_1/c} + T_{\Delta x}^{c_{-1}/c} \right) + \frac{u}{c} \left(T_{\Delta x}^{c_1/c} - T_{\Delta x}^{c_{-1}/c} \right) - \frac{u^2}{c^2} \left(2T_{\Delta x}^{c_1/c} - 4T_{\Delta x}^{c_0/c} + 2T_{\Delta x}^{c_{-1}/c} \right) \right) & \dots \\ \frac{c s_1}{2} \left(\left(T_{\Delta x}^{c_1/c} - T_{\Delta x}^{c_{-1}/c} \right) - \frac{u^2}{c^2} \left(3T_{\Delta x}^{c_1/c} - 3T_{\Delta x}^{c_{-1}/c} \right) + \frac{u^3}{c^3} \left(2T_{\Delta x}^{c_1/c} - 4T_{\Delta x}^{c_0/c} + 2T_{\Delta x}^{c_{-1}/c} \right) \right) & & \\ \dots & \frac{s_2}{2c^2} \left(T_{\Delta x}^{c_1/c} - 2T_{\Delta x}^{c_0/c} + T_{\Delta x}^{c_{-1}/c} \right) & \\ \dots & \frac{s_2}{2c} \left(\left(T_{\Delta x}^{c_1/c} - T_{\Delta x}^{c_{-1}/c} \right) - \frac{u}{c} \left(T_{\Delta x}^{c_1/c} - 2T_{\Delta x}^{c_0/c} + T_{\Delta x}^{c_{-1}/c} \right) \right) & \\ \frac{s_2}{2} \left(\left(T_{\Delta x}^{c_1/c} + T_{\Delta x}^{c_{-1}/c} \right) - \frac{u}{c} \left(T_{\Delta x}^{c_1/c} - T_{\Delta x}^{c_{-1}/c} \right) + \frac{u^2}{c^2} \left(T_{\Delta x}^{c_1/c} - 2T_{\Delta x}^{c_0/c} + T_{\Delta x}^{c_{-1}/c} \right) \right) & & \end{pmatrix}. \quad (22) \end{aligned}$$

The characteristic polynomial \mathcal{X}_P of the matrix P is written as:

$$\mathcal{X}_P = \gamma_3 X^3 + \gamma_2 X^2 + \gamma_1 X + \gamma_0 I, \quad (23)$$

where the coefficients γ_i in Eq. (23) are given by:

$$\gamma_3 = T_{\Delta x}^{c_0/c}, \quad (24a)$$

$$\begin{aligned} \gamma_2 &= \frac{s_0}{2} \left(2T_{\Delta x}^{c_0/c} + \frac{u}{c} \left(T_{\Delta x}^{c_1/c} - T_{\Delta x}^{c_{-1}/c} \right) + \frac{u^2}{c^2} \left(T_{\Delta x}^{c_1/c} - 2T_{\Delta x}^{c_0/c} + T_{\Delta x}^{c_{-1}/c} \right) \right) \\ &+ \frac{s_1}{2} \left(\left(T_{\Delta x}^{c_1/c} + T_{\Delta x}^{c_{-1}/c} \right) + \frac{u}{c} \left(T_{\Delta x}^{c_1/c} - T_{\Delta x}^{c_{-1}/c} \right) - 2 \frac{u^2}{c^2} \left(T_{\Delta x}^{c_1/c} - 2T_{\Delta x}^{c_0/c} + T_{\Delta x}^{c_{-1}/c} \right) \right) \\ &+ \frac{s_2}{2} \left(\left(T_{\Delta x}^{c_1/c} + T_{\Delta x}^{c_{-1}/c} \right) - 2 \frac{u}{c} \left(T_{\Delta x}^{c_1/c} - T_{\Delta x}^{c_{-1}/c} \right) + \frac{u^2}{c^2} \left(T_{\Delta x}^{c_1/c} - 2T_{\Delta x}^{c_0/c} + T_{\Delta x}^{c_{-1}/c} \right) \right) \\ &- \left(T_{\Delta x}^{c_1/c} + T_{\Delta x}^{c_0/c} + T_{\Delta x}^{c_{-1}/c} \right), \quad (24b) \end{aligned}$$

$$\begin{aligned}
\gamma_1 = & \frac{s_0}{2} \left(-2 \left(T_{\Delta x}^{c_1/c} + T_{\Delta x}^{c_{-1}/c} \right) - \frac{u}{c} \left(T_{\Delta x}^{c_1/c} - T_{\Delta x}^{c_{-1}/c} \right) + \frac{u^2}{c^2} \left(T_{\Delta x}^{c_1/c} - 2 T_{\Delta x}^{c_0/c} + T_{\Delta x}^{c_{-1}/c} \right) \right) \\
& + s_1 \left(\left(T_{\Delta x}^{c_1/c} + T_{\Delta x}^{c_{-1}/c} \right) + 2 \frac{u}{c} \left(T_{\Delta x}^{c_1/c} - T_{\Delta x}^{c_{-1}/c} \right) + \frac{u^2}{c^2} \left(T_{\Delta x}^{c_1/c} - 2 T_{\Delta x}^{c_0/c} + T_{\Delta x}^{c_{-1}/c} \right) \right) \\
& + s_2 \left(\left(T_{\Delta x}^{c_1/c} + T_{\Delta x}^{c_{-1}/c} \right) - \frac{u}{c} \left(T_{\Delta x}^{c_1/c} - T_{\Delta x}^{c_{-1}/c} \right) - \frac{u^2}{c^2} \left(T_{\Delta x}^{c_1/c} - 2 T_{\Delta x}^{c_0/c} + T_{\Delta x}^{c_{-1}/c} \right) \right) \\
& + \frac{s_1 s_2}{2} \left(2 T_{\Delta x}^{c_0/c} - \frac{u}{c} \left(T_{\Delta x}^{c_1/c} - T_{\Delta x}^{c_{-1}/c} \right) + \frac{u^2}{c^2} \left(T_{\Delta x}^{c_1/c} - 2 T_{\Delta x}^{c_0/c} + T_{\Delta x}^{c_{-1}/c} \right) \right) \\
& - \frac{s_1}{2} \left(\left(T_{\Delta x}^{c_1/c} + 2 T_{\Delta x}^{c_0/c} + T_{\Delta x}^{c_{-1}/c} \right) + \frac{u}{c} \left(T_{\Delta x}^{c_1/c} - T_{\Delta x}^{c_{-1}/c} \right) + \frac{u^2}{c^2} \left(T_{\Delta x}^{c_1/c} - 2 T_{\Delta x}^{c_0/c} + T_{\Delta x}^{c_{-1}/c} \right) \right) \\
& - \frac{s_2}{2} \left(\left(T_{\Delta x}^{c_1/c} + 2 T_{\Delta x}^{c_0/c} + T_{\Delta x}^{c_{-1}/c} \right) - \frac{u}{c} \left(T_{\Delta x}^{c_1/c} - T_{\Delta x}^{c_{-1}/c} \right) - \frac{u^2}{c^2} \left(T_{\Delta x}^{c_1/c} - 2 T_{\Delta x}^{c_0/c} + T_{\Delta x}^{c_{-1}/c} \right) \right) \\
& + \left(T_{\Delta x}^{c_1/c} + T_{\Delta x}^{c_0/c} + T_{\Delta x}^{c_{-1}/c} \right), \\
\gamma_0 = & -(1 - s_0)(1 - s_1)(1 - s_2) T_{\Delta x}^{c_0/c}.
\end{aligned} \tag{24c}$$

Note, the coefficients γ_i in Eq. (24) are simplified based on the following identities: $T_{\Delta x}^{c_1/c} T_{\Delta x}^{c_{-1}/c} = T_{\Delta x}^{c_0/c}$, $T_{\Delta x}^{c_1/c} T_{\Delta x}^{c_0/c} = T_{\Delta x}^{c_1/c}$, $T_{\Delta x}^{c_{-1}/c} T_{\Delta x}^{c_0/c} = T_{\Delta x}^{c_{-1}/c}$. As the final step in the derivation, we expand the indices in Eq. (19) and substitute the γ_i coefficients given in Eq. (24), the T , P and Q matrices given in Eqs. (20), (21) and (22), respectively, and the $\{m^{\text{eq}}\}$ equilibrium moments in the CM space given by Eq. (9). Lastly, we make use of the definition $T_{\Delta x}^{c_k/c} [\phi_j] = \phi_{j-c_k/c}$ to arrive at the equivalent finite difference (EFD) scheme satisfied by the LBM with the MRT-CM collision operator for the 1D time-dependent ADE. This EFD is expressed by a *four-level finite-difference* (FLFD) equation on the conservative variable ϕ as follows:

$$\phi_j^{n+1} = \alpha_1 \phi_j^n + \alpha_2 \phi_{j-1}^n + \alpha_3 \phi_{j+1}^n + \beta_1 \phi_j^{n-1} + \beta_2 \phi_{j-1}^{n-1} + \beta_3 \phi_{j+1}^{n-1} + \gamma \phi_j^{n-2}, \tag{25}$$

with coefficients:

$$\alpha_1 = 1 - s_2 \left(1 - w_0 + \frac{u^2}{c^2} \right) - 2(s_1 - s_2) \frac{u^2}{c^2}, \tag{26a}$$

$$\alpha_2 = 1 - \frac{s_1}{2} \left(1 - \frac{u}{c} \right) - \frac{s_2}{2} + \frac{s_2}{2} \left(1 - w_0 + \frac{u^2}{c^2} \right) - (s_1 - s_2) \left(\frac{u}{c} - \frac{u^2}{c^2} \right), \tag{26b}$$

$$\alpha_3 = 1 - \frac{s_1}{2} \left(1 + \frac{u}{c} \right) - \frac{s_2}{2} + \frac{s_2}{2} \left(1 - w_0 + \frac{u^2}{c^2} \right) - (s_1 - s_2) \left(-\frac{u}{c} - \frac{u^2}{c^2} \right), \tag{26c}$$

$$\beta_1 = (1 - s_1) \left(-1 + s_2 - s_2 \left(1 - w_0 + \frac{u^2}{c^2} \right) \right) - 2(s_1 - s_2) \frac{u^2}{c^2}, \tag{26d}$$

$$\beta_2 = (1 - s_2) \left(\frac{s_1}{2} \left(1 - \frac{u}{c} \right) - 1 \right) - \frac{s_2}{2} (1 - s_1) + \frac{s_2}{2} (1 - s_1) \left(1 - w_0 + \frac{u^2}{c^2} \right) + (s_1 - s_2) \left(\frac{u}{c} + \frac{u^2}{c^2} \right), \tag{26e}$$

$$\beta_3 = (1 - s_2) \left(\frac{s_1}{2} \left(1 + \frac{u}{c} \right) - 1 \right) - \frac{s_2}{2} (1 - s_1) + \frac{s_2}{2} (1 - s_1) \left(1 - w_0 + \frac{u^2}{c^2} \right) + (s_1 - s_2) \left(-\frac{u}{c} + \frac{u^2}{c^2} \right), \tag{26f}$$

$$\gamma = (1 - s_1) (1 - s_2). \tag{26g}$$

Remark 1. The underlined terms in Eq. (26) denote the terms specific to the central moment (CM) collision model. Without the underlined terms, the FLFD coefficients given by Eq. (26) coincide with those of the MRT-RM scheme, i.e. formulated on the resting frame, for the 1D time-dependent ADE derived in [61]; this can be confirmed by comparing our Eq. (26) against Eq. (23) of Chen et al. work [61].

According to the FLFD representation of the CM-LBM scheme, it is possible to point out the following observations.

First, when the single-relaxation-time BGK collision model is adopted, i.e. $s_1 = s_2 = s$, the LBM formulated on RM or CM spaces becomes exactly equivalent. This theoretical conclusion is in agreement with previous works [29,30], which pointed out this equivalency based on numerical evidence. At the same time, it also questions other works [25,67] that considered the BGK formulated on the CM space as a distinct collision model, which as shown here ends up recovering the LBM-BGK in its traditional form [8].

Second, it is evident that, when $u = 0$, the RM and CM discretizations are the same and reduce to the FLFD scheme for the diffusion equation. In fact, the coefficients of FLFD scheme in Eq. (26) with $u = 0$ recover those previously published in [54,57,58]. This observation proves that it is senseless to apply the CM space formulation in the modelling of pure diffusive problems.

Third, as expected, the relaxation rate s_0 associated with the relaxation of the zeroth-order moment, i.e. the conserved mode $m_0 = \phi$, does not impact the FLFD equation as shown by the coefficients in Eq. (26). Conversely, besides the relaxation parameter s_1 associated with the relaxation of the first-order moment, which controls the diffusion coefficient D , see Eq. (36), also the relaxation parameter s_2 associated with the relaxation of the second-order moment, which does not have any direct relation with physics, impacts the coefficients of the FLFD equation in Eq. (26) for the ADE, Eq. (1).

4. Steady-state difference scheme

For the time-independent regime, we drop the index n from the ϕ variable in Eq. (25), multiply each term by $1/(\Delta t s_1 s_2)$, and group the results into common terms. After a few manipulations, we obtain the EFD scheme of the CM-LBM for the steady-state ADE:

$$u \left(\frac{\phi_{j+1} - \phi_{j-1}}{2 \Delta x} \right) = D_{\text{eff}} \left(\frac{\phi_{j+1} - 2\phi_j + \phi_{j-1}}{\Delta x^2} \right). \tag{27}$$

The effective diffusion coefficient D_{eff} in Eq. (27) depends on the LBM model details, namely: (i) the collision model adopted, and (ii) whether equilibrium is expanded to first-order (i.e. $\eta = 0$ in Eq. (5)) or to second-order (i.e. $\eta = 2(1 - \omega_0)/\omega_0$ in Eq. (5)). According to each modelling

scenario, the D_{eff} coefficient reads:

$$D_{\text{eff}} = \begin{cases} \left(1 - \omega_0 + \frac{u^2}{c^2}\right) c^2 \Lambda_1 \Delta t, & \text{MRT-RM with quadratic equilibrium} \\ \left(1 - \omega_0 + \frac{u^2}{c^2} + 2 \left(\frac{\Lambda_2}{\Lambda_1} - 1\right) \frac{u^2}{c^2}\right) c^2 \Lambda_1 \Delta t, & \text{MRT-CM with quadratic equilibrium} \\ (1 - \omega_0) c^2 \Lambda_1 \Delta t, & \text{MRT-RM with linear equilibrium} \\ \left(1 - \omega_0 + 2 \left(\frac{\Lambda_2}{\Lambda_1} - 1\right) \frac{u^2}{c^2}\right) c^2 \Lambda_1 \Delta t, & \text{MRT-CM with linear equilibrium} \end{cases} \quad (28)$$

where $\Lambda_1 = \left(\frac{1}{s_1} - \frac{1}{2}\right)$ and $\Lambda_2 = \left(\frac{1}{s_2} - \frac{1}{2}\right)$. A closer inspection of Eq. (27) with diffusion coefficient D_{eff} based on Eq. (28) permits extracting the following observations.

First, in consistency with the notation introduced in Section 3 the underlined terms in Eq. (28) denote the specific terms introduced by the central moment (CM) space collision model. Without the underlined terms, the effective diffusion coefficient in Eq. (28) recovers the same D_{eff} structure of the MRT-RM model, also shown in previous works [52,68,69].

Second, except for the MRT-RM model running with the linear equilibrium, all other combinations in Eq. (28) introduce a u^2 -dependent error term in the modelled diffusion coefficient D_{eff} . Such an u^2 dependency on D_{eff} is a well-known numerical artefact in the LBM modelling of the steady ADE [68,69] and typically can be avoided with the use of the linear equilibrium. It turns out that the MRT-CM with quadratic equilibrium can also eliminate this u^2 artefact with the relaxation combination $s_2 = \frac{4s_1}{2+s_1}$. On the other hand, to achieve the same goal, the MRT-CM with linear equilibrium requires $s_2 = s_1$, a case where the MRT-CM model reduces to the standard BGK model (recall Section 3).

Finally, let us analyse the LBM models presented above and solve the steady discrete ADE, Eq. (27), subject to boundary conditions $\phi(-L/2) = \phi_0$ and $\phi(L/2) = \phi_L$, so that the exact discrete solution, $\phi_j := \phi(x_j)$, is obtained as follows:

$$\phi_j = \phi_0 + (\phi_L - \phi_0) \frac{1 - \mathcal{R}^{\frac{L}{2} + x_j}}{1 - \mathcal{R}^L} \quad \text{with} \quad \mathcal{R} = \frac{2 + \text{Pe}_{\Delta x}}{2 - \text{Pe}_{\Delta x}} \quad \text{and} \quad \text{Pe}_{\Delta x} = \frac{u \Delta x}{D_{\text{eff}}}. \quad (29)$$

Note that, for grid Péclet numbers $|\text{Pe}_{\Delta x}| > 2$ the discrete solution ϕ_j becomes complex, except at grid nodes x_j , which leads to a solution with wiggles. For comparison purposes, the continuum analytical solution of this problem is given by:

$$\phi(x) = \phi_0 + (\phi_L - \phi_0) \frac{1 - e^{\text{Pe}(\frac{1}{2} + \frac{x}{L})}}{1 - e^{\text{Pe}}} \quad \text{with} \quad \text{Pe} = \frac{uL}{D}. \quad (30)$$

Fig. 1 displays analytical versus numerical ϕ solutions at small, moderate and large Péclet regimes, respectively given by $\text{Pe} = \{1, 10, 100\}$. For the most critical case $\text{Pe} = 100$, where the right boundary layer is under-resolved, the parameter combination $s_1 = 1.2$, $s_2 = 0.9$ and $\omega_0 = 2/3$ seems to indicate that the MRT-CM model with linear equilibrium reaches the best accuracy. However, this conclusion is not universal. For example, other combinations of s_1 , s_2 and ω_0 will alter the D_{eff} value in Eq. (27) and potentially suggest that a different collision model and equilibrium combination may reach a better accuracy. This lack of universality hints for the adoption of a different criterion to guide in the best choice for collision/equilibrium model, rather than accuracy alone. To this end, we note that, at steady-state, the dimensionless ADE is solely governed by the Péclet number, see Eq. (30). So, to be consistent with this physical scaling requirement, the corresponding discrete approximation, Eq. (27), should reproduce this same Pe number parameterization. It turns out that such a parameterization property fails to be satisfied whenever the D_{eff} coefficient in Eq. (27) features u^2 dependencies. In light of this criterion, the suitable combination for this problem class is the MRT-RM collision model with the linear equilibrium since this is the only model guaranteeing that the LBM steady solution is solely controlled by Pe, regardless the individual D and u values adopted [44]. Moreover, the CM space formulation, regardless the equilibrium used, does not seem suitable to model the steady ADE.

5. Accuracy analysis of the EFD scheme

This section presents the accuracy analysis for the four-level finite difference (FLFD) scheme derived in Eqs. (25) and (26). The goal of our accuracy analysis is twofold. First, we intend to reveal the structure of the leading order truncation errors of the LBM with different collision operators (MRT-CM, MRT-RM, REG and BGK models) in the approximation of the time-dependent 1D ADE. Second, we search for the suitable combinations in the model parameters of each collision scheme that lead to an enhanced accuracy. Below, the main steps of the accuracy analysis are summarized, which follow the presentation style of the works [57–59,61–63].

First, consider the Taylor series of ϕ about the position $x_j = j \Delta x$ and time $t_n = n \Delta t$, defined as follows:

$$\phi(x_j + k \Delta x, t_n + m \Delta t) = \phi(x_j, t_n) + \sum_{r=1}^o \frac{1}{r!} \sum_{s=0}^r \binom{r}{s} (k \Delta x)^s (m \Delta t)^{s-r} \frac{\partial^r \phi}{\partial x^r} \Big|_{(x_j, t_n)} \quad (31)$$

where $\binom{r}{s} = \frac{r!}{(r-s)! s!}$ is the binomial coefficient.

Next, let us apply this Taylor series expansion up to fourth order ($o = 4$) [Eq. (31)] over each term in Eq. (25), and subsequently group the resulting terms into common coefficients. After some algebraic manipulations, we obtain:

$$(1 + \beta_1 + \beta_2 + \beta_3 + 2\gamma) \left[\frac{\partial \phi}{\partial t} \right]_j^n + (\alpha_2 - \alpha_3 + \beta_2 - \beta_3) \frac{\Delta x}{\Delta t} \left[\frac{\partial \phi}{\partial x} \right]_j^n = \frac{1}{2} (\alpha_2 + \alpha_3 + \beta_2 + \beta_3) \frac{\Delta x^2}{\Delta t} \left[\frac{\partial^2 \phi}{\partial x^2} \right]_j^n + \text{TE} \quad (32)$$

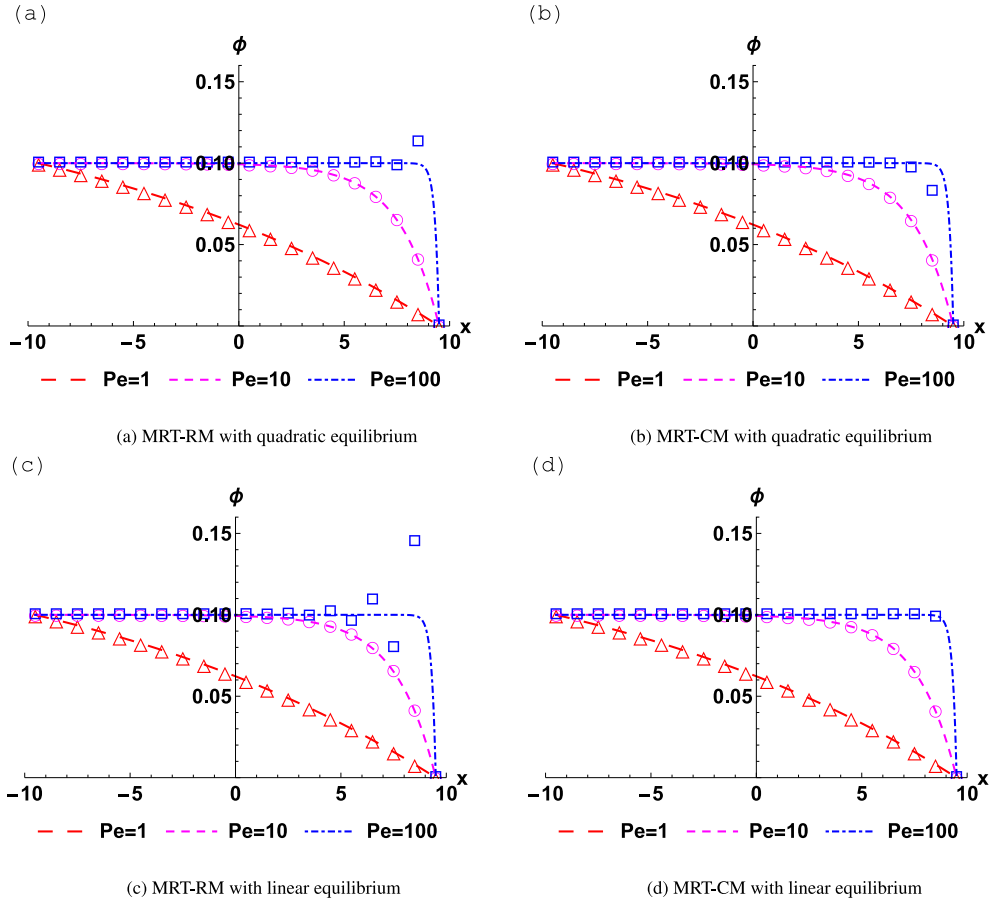


Fig. 1. Steady state ADE solution as function of the Péclet number $Pe = \frac{uL}{D}$ with the following numerical parameters: $L = N_x$, $\Delta x = 20$, $s_1 = 1.2$, $s_2 = 0.9$, $\omega_0 = 2/3$. Continuous lines: PDE analytical solutions. Markers: LBM discrete solutions. Accuracies for the most critical case, $Pe = 100$: Panel (a) $L_2 = 0.0312727$; Panel (b) $L_2 = 0.0392397$; Panel (c) $L_2 = 0.116462$; Panel (d) $L_2 = 0.00217795$. The L_2 measure is defined in Eq. (67).

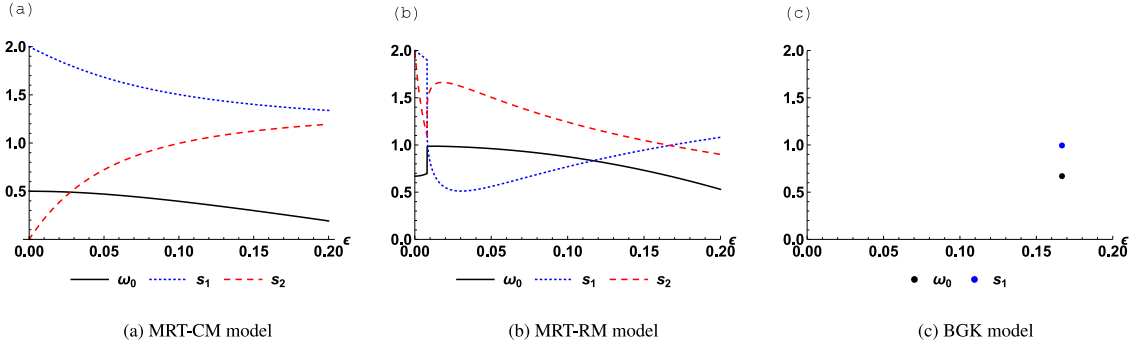


Fig. 2. 4th order accurate solution $\{\omega_0, s_1, s_2\}$ for $u/c = 0.1$. Although multiple solutions exist, the curves/points here depicted represent one of them. Recall, $\epsilon = (1 - \omega_0)A_1$, $s_1 = 2/(1 + 2A_1)$ and $s_2 = 2/(1 + 2A_2)$.

with the truncation error TE given by:

$$\begin{aligned}
 TE = & (\beta_2 - \beta_3) \Delta x \left[\frac{\partial^2 \phi}{\partial x \partial t} \right]_j^n + \frac{1}{2} (-1 + \beta_1 + \beta_2 + \beta_3 + 4\gamma) \Delta t \left[\frac{\partial^2 \phi}{\partial t^2} \right]_j^n + \frac{1}{6} (-\alpha_2 + \alpha_3 - \beta_2 + \beta_3) \frac{\Delta x^3}{\Delta t} \left[\frac{\partial^3 \phi}{\partial x^3} \right]_j^n \\
 & - \frac{1}{2} (\beta_2 - \beta_3) \Delta x \Delta t \left[\frac{\partial^3 \phi}{\partial x \partial t^2} \right]_j^n - \frac{1}{2} (\beta_2 + \beta_3) \Delta x^2 \left[\frac{\partial^3 \phi}{\partial x^2 \partial t} \right]_j^n - \frac{1}{6} (1 + \beta_1 + \beta_2 + \beta_3 + 8\gamma) \Delta t^2 \left[\frac{\partial^3 \phi}{\partial t^3} \right]_j^n \\
 & + \frac{1}{24} (\alpha_2 + \alpha_3 + \beta_2 + \beta_3) \frac{\Delta x^4}{\Delta t} \left[\frac{\partial^4 \phi}{\partial x^4} \right]_j^n + \frac{1}{6} (\beta_2 - \beta_3) \Delta x \Delta t^2 \left[\frac{\partial^4 \phi}{\partial x \partial t^3} \right]_j^n + \frac{1}{4} (\beta_2 + \beta_3) \Delta x^2 \Delta t \left[\frac{\partial^4 \phi}{\partial x^2 \partial t^2} \right]_j^n \\
 & + \frac{1}{6} (\beta_2 - \beta_3) \Delta x^3 \left[\frac{\partial^4 \phi}{\partial x^3 \partial t} \right]_j^n + \frac{1}{24} (-1 + \beta_1 + \beta_2 + \beta_3 + 16\gamma) \Delta t^3 \left[\frac{\partial^4 \phi}{\partial t^4} \right]_j^n + \dots
 \end{aligned} \tag{33}$$

Now, let us introduce the target differential equation, $\left[\frac{\partial\phi}{\partial t}\right]_j^n + u \left[\frac{\partial\phi}{\partial x}\right]_j^n = D \left[\frac{\partial^2\phi}{\partial x^2}\right]_j^n$, and derive the following relations:

$$\begin{aligned}
\left[\frac{\partial^2\phi}{\partial x\partial t}\right]_j^n &= D \left[\frac{\partial^3\phi}{\partial x^3}\right]_j^n - u \left[\frac{\partial^2\phi}{\partial x^2}\right]_j^n + \mathcal{O}(\Delta x^3, \Delta t \Delta x) \\
\left[\frac{\partial^2\phi}{\partial t^2}\right]_j^n &= D^2 \left[\frac{\partial^4\phi}{\partial x^4}\right]_j^n - 2Du \left[\frac{\partial^3\phi}{\partial x^3}\right]_j^n + u^2 \left[\frac{\partial^2\phi}{\partial x^2}\right]_j^n + \mathcal{O}(\Delta t) \\
\left[\frac{\partial^3\phi}{\partial x\partial t^2}\right]_j^n &= -2Du \left[\frac{\partial^4\phi}{\partial x^4}\right]_j^n + u^2 \left[\frac{\partial^3\phi}{\partial x^3}\right]_j^n + \mathcal{O}(\Delta x) \\
\left[\frac{\partial^3\phi}{\partial x^2\partial t}\right]_j^n &= D \left[\frac{\partial^4\phi}{\partial x^4}\right]_j^n - u \left[\frac{\partial^3\phi}{\partial x^3}\right]_j^n + \mathcal{O}\left(\frac{\Delta x^4}{\Delta t}, \Delta x^2\right) \\
\left[\frac{\partial^3\phi}{\partial t^3}\right]_j^n &= 3Du^2 \left[\frac{\partial^4\phi}{\partial x^4}\right]_j^n - u^3 \left[\frac{\partial^3\phi}{\partial x^3}\right]_j^n + \mathcal{O}\left(\frac{\Delta x^2}{\Delta t}\right) \\
\left[\frac{\partial^4\phi}{\partial x\partial t^3}\right]_j^n &= -u^3 \left[\frac{\partial^4\phi}{\partial x^4}\right]_j^n + \mathcal{O}\left(\frac{1}{\Delta x}\right) \\
\left[\frac{\partial^4\phi}{\partial x^3\partial t}\right]_j^n &= -u \left[\frac{\partial^4\phi}{\partial x^4}\right]_j^n + \mathcal{O}(\Delta x) \\
\left[\frac{\partial^4\phi}{\partial x^2\partial t^2}\right]_j^n &= u^2 \left[\frac{\partial^4\phi}{\partial x^4}\right]_j^n + \mathcal{O}\left(\frac{\Delta x^2}{\Delta t}\right) \\
\left[\frac{\partial^4\phi}{\partial t^4}\right]_j^n &= u^4 \left[\frac{\partial^4\phi}{\partial x^4}\right]_j^n + \mathcal{O}\left(\frac{1}{\Delta t}\right)
\end{aligned} \tag{34}$$

Eqs. (34) enable us to replace both the time derivative terms and the mixed time and space derivative terms appearing on the right-hand side of Eq. (33) by equivalent terms only involving spatial derivatives. By doing so, we obtain:

$$\begin{aligned}
&(1 + \beta_1 + \beta_2 + \beta_3 + 2\gamma) \left[\frac{\partial\phi}{\partial t}\right]_j^n + (\alpha_2 - \alpha_3 + \beta_2 - \beta_3) \frac{\Delta x}{\Delta t} \left[\frac{\partial\phi}{\partial x}\right]_j^n = \\
&\left[\frac{1}{2}(\alpha_2 + \alpha_3 + \beta_2 + \beta_3) \frac{\Delta x^2}{\Delta t} - u(\beta_2 - \beta_3) \Delta x + \frac{1}{2}u^2(-1 + \beta_1 + \beta_2 + \beta_3 + 4\gamma) \Delta t\right] \left[\frac{\partial^2\phi}{\partial x^2}\right]_j^n \\
&+ \left[\frac{1}{6}(-\alpha_2 + \alpha_3 - \beta_2 + \beta_3) \frac{\Delta x^3}{\Delta t} + D(\beta_2 - \beta_3) \Delta x - Du(-1 + \beta_1 + \beta_2 + \beta_3 + 4\gamma) \Delta t\right. \\
&\quad \left. - \frac{1}{2}u^2(\beta_2 - \beta_3) \Delta x \Delta t + \frac{1}{2}u(\beta_2 + \beta_3) \Delta x^2 + \frac{1}{6}u^3(1 + \beta_1 + \beta_2 + \beta_3 + 8\gamma) \Delta t^2\right] \left[\frac{\partial^3\phi}{\partial x^3}\right]_j^n \\
&+ \left[\frac{1}{24}(\alpha_2 + \alpha_3 + \beta_2 + \beta_3) \frac{\Delta x^4}{\Delta t} + \frac{1}{2}D^2(-1 + \beta_1 + \beta_2 + \beta_3 + 4\gamma) \Delta t + Du(\beta_2 - \beta_3) \Delta x \Delta t\right. \\
&\quad \left. - \frac{1}{2}D(\beta_2 + \beta_3) \Delta x^2 - \frac{1}{2}Du^2(1 + \beta_1 + \beta_2 + \beta_3 + 8\gamma) \Delta t^2 - \frac{1}{6}u^3(\beta_2 - \beta_3) \Delta x \Delta t^2\right. \\
&\quad \left. + \frac{1}{4}u^2(\beta_2 + \beta_3) \Delta x^2 \Delta t - \frac{1}{6}u(\beta_2 - \beta_3) \Delta x^3 + \frac{1}{24}u^4(-1 + \beta_1 + \beta_2 + \beta_3 + 16\gamma) \Delta t^3\right] \left[\frac{\partial^4\phi}{\partial x^4}\right]_j^n + \dots
\end{aligned} \tag{35}$$

where the diffusion coefficient is

$$D = (1 - \omega_0) c^2 \left(\frac{1}{s_1} - \frac{1}{2}\right) \Delta t. \tag{36}$$

In what follows, it is instructive to introduce the relaxation functions $\Lambda_1 = \left(\frac{1}{s_1} - \frac{1}{2}\right)$, $\Lambda_2 = \left(\frac{1}{s_2} - \frac{1}{2}\right)$ and $\Lambda = \Lambda_1 \Lambda_2$. Then, after some algebraic manipulations, we arrive at the equivalent partial differential equation (EPDE) reproduced by the LBM model for the 1D ADE:

$$\left[\frac{\partial\phi}{\partial t}\right]_j^n + u \left[\frac{\partial\phi}{\partial x}\right]_j^n = D \left[\frac{\partial^2\phi}{\partial x^2}\right]_j^n + u \Delta x^2 \text{TE}_3 \left[\frac{\partial^3\phi}{\partial x^3}\right]_j^n + \frac{\Delta x^4}{\Delta t} \text{TE}_4 \left[\frac{\partial^4\phi}{\partial x^4}\right]_j^n + \dots \tag{37}$$

where the leading-order truncation errors for advection TE_3 and diffusion TE_4 have distinct structures according to the LBM collision model.

1. Truncation errors in the MRT-CM model:

$$\text{TE}_3^{\text{MRT-CM}} = \left(2 - 3\omega_0 + \frac{u^2}{c^2}\right) \left(\Lambda - \frac{1}{12}\right), \tag{38a}$$

$$\begin{aligned}
\text{TE}_4^{\text{MRT-CM}} &= (1 - \omega_0) \Lambda_1 \left(\omega_0 \left(\Lambda - \frac{1}{6}\right) - (1 - \omega_0) \left(\Lambda_1^2 - \frac{1}{12}\right)\right) \\
&\quad + \frac{u^2}{c^2} \left(\frac{1}{2}(2 - 3\omega_0) \left(\Lambda - \frac{1}{2}\Lambda_1 - \frac{1}{12}\right) - 3(1 - \omega_0)\Lambda_1 \left(\Lambda - \frac{1}{6}\right)\right) \\
&\quad + \frac{u^4}{c^4} \left(\frac{1}{2} \left(\Lambda - \frac{1}{2}\Lambda_1 - \frac{1}{12}\right)\right).
\end{aligned} \tag{38b}$$

2. Truncation errors in the MRT-RM model (determined by repeating the above analysis, but omitting the underlined terms in Eq. (26)):

$$\text{TE}_3^{\text{MRT-RM}} = 2(1 - \omega_0) \left(\Lambda_1^2 - \frac{1}{12}\right) - \left(\omega_0 - \frac{u^2}{c^2}\right) \left(\Lambda - \frac{1}{12}\right), \tag{39a}$$

$$\begin{aligned} \text{TE}_4^{\text{MRT-RM}} = & (1 - \omega_0) A_1 \left(\omega_0 \left(\Lambda - \frac{1}{6} \right) - (1 - \omega_0) \left(\Lambda_1^2 - \frac{1}{12} \right) \right) \\ & + \frac{u^2}{c^2} \left(\frac{1}{2} (2 - 3\omega_0) \left(\Lambda - \frac{1}{2} A_1 - \frac{1}{12} \right) - 3(1 - \omega_0) A_1 \left(\Lambda - \frac{1}{6} \right) - (1 - \omega_0) (\Lambda - \Lambda_1^2) + \frac{1}{6A_1} (\Lambda - \Lambda_1^2) \right) \\ & + \frac{u^4}{c^4} \left(\frac{1}{2} \left(\Lambda - \frac{1}{12} \right) - \frac{1}{6A_1} \left(\Lambda + \frac{1}{2} \Lambda_1^2 \right) \right). \end{aligned} \quad (39b)$$

3. Truncation errors in the REG model (determined by setting $\Lambda = \frac{1}{2} A_1$ and $A_2 = \frac{1}{2}$ in Eqs. (39a) and (39b)):

$$\text{TE}_3^{\text{REG}} = 2(1 - \omega_0) \left(\Lambda_1^2 - \frac{1}{12} \right) - \left(\omega_0 - \frac{u^2}{c^2} \right) \left(\frac{1}{2} A_1 - \frac{1}{12} \right), \quad (40a)$$

$$\begin{aligned} \text{TE}_4^{\text{REG}} = & (1 - \omega_0) A_1 \left(\frac{1}{2} \omega_0 \left(A_1 - \frac{1}{3} \right) - (1 - \omega_0) \left(\Lambda_1^2 - \frac{1}{12} \right) \right) \\ & + \frac{u^2}{c^2} \left(\frac{1}{2} (\omega_0 - 1) \left(\Lambda_1^2 + \frac{1}{4} \right) - \frac{1}{6} \left(A_1 - \frac{3}{4} \right) \right) \\ & + \frac{u^4}{c^4} \left(\frac{1}{6} \left(A_1 - \frac{3}{4} \right) \right). \end{aligned} \quad (40b)$$

4. Truncation errors in the BGK model (determined by setting $\Lambda = \Lambda_1^2$ and $A_2 = A_1$ in Eqs. (39a) and (39b)):

$$\text{TE}_3^{\text{BGK}} = \left(2 - 3\omega_0 + \frac{u^2}{c^2} \right) \left(\Lambda_1^2 - \frac{1}{12} \right), \quad (41a)$$

$$\begin{aligned} \text{TE}_4^{\text{BGK}} = & (1 - \omega_0) A_1 \left(\frac{1}{2} \omega_0 \left(\Lambda_1^2 - \frac{1}{8} \right) - \left(\Lambda_1^2 - \frac{1}{12} \right) \right) \\ & + \frac{u^2}{c^2} \left(3\omega_0 \left(\Lambda_1^3 - \frac{1}{2} \Lambda_1^2 + \frac{1}{4} A_1 + \frac{1}{24} \right) - 3\Lambda_1^3 + \Lambda_1^2 - \frac{1}{12} \right) \\ & + \frac{u^4}{c^4} \left(\frac{1}{2} \left(\Lambda_1^2 - \frac{1}{2} A_1 - \frac{1}{12} \right) \right). \end{aligned} \quad (41b)$$

Based on the structure of the TE_3 and TE_4 errors in each collision model, the following conclusions can be outlined.

First, it is confirmed that the leading-order truncation errors of the MRT-RM model, given by Eqs. (39a) and (39b), coincide with Eq. (28) by Chen et al. [61] (although last term in Eq. (28c) of [61] has a typo and it should read as $s_1^2(6 - 5s_1 - 4s_2 + 5\frac{s_1 s_2}{2})$). Our Eqs. (39) also agree with Eqs. (2.9) and (2.10) by Ginzburg [45], which followed a different theoretical framework based on the recurrence equations method [44].

Second, looking at the dependence of truncation errors on the relaxation parameters, it is found that MRT models depend on both Λ and A_1 (and their products). On the other hand, since the REG and BGK models are subsets of the MRT-RM, their truncation errors dependency is on A_1 only. Bearing in mind that A_1 determines the D diffusion coefficient, see Eq. (36), and considering the presence of A_1 on each model, it can be concluded that the undesirable non-linear impact of D on numerical errors will be worse on BGK, followed by REG, and less impactful on MRT models. It is important to note that, unlike the steady-state case, the time-dependent solutions in LBM inevitably have part of the numerical errors depending on the transport coefficients. Such a D -dependence on numerical errors happens regardless of the collision model [44,45,70].

Third, within the MRT models, the CM space formulation recovers much more compact truncation error terms, which exhibit a weaker dependence on the undesirable contribution A_1 when compared to the RM space formulation. In fact, the third-order numerical error $\text{TE}_3^{\text{MRT-CM}}$ is vanished for $\Lambda = \frac{1}{12}$, which is exactly the ‘‘optimal advection’’ condition satisfied by the steady-state settings of the MRT-RM and TRT models. Due to this equivalence, it can be inferred that the CM space formulation is able to eliminate the leading order error terms with a time-dependent origin, which act as the leading advection corrections in the truncation terms. This fact justifies why the MRT-CM model is able to improve the Galilean invariance of this numerical scheme, at least, on the leading-order error [27].

Fourth, according to Eq. (37), the LBM approximates the time-dependent ADE, Eq. (1), with second-order accuracy under the diffusive scaling $\Delta t \propto \Delta x^2$. Fourth-order accuracy may be achieved when the following two conditions are simultaneously met: $\text{TE}_3 = 0$ and $\text{TE}_4 = 0$. Such an ‘‘optimal advection-diffusion’’ condition can be satisfied with a proper choice of the free parameters ω_0 , s_1 and s_2 , giving the fixed conditions u/c and ϵ (where $\epsilon = D \Delta t / \Delta x^2$); note that their ratio defines the grid Péclet number $\text{Pe}_{\Delta x} = \frac{u/c}{\epsilon} = \frac{u \Delta x}{D}$. Finding the values of ω_0 , s_1 and s_2 that set $\text{TE}_3 = 0$ and $\text{TE}_4 = 0$ typically requires solving a non-linear problem and the obtained solution may not be unique. Fig. 2 illustrates one possible solution for the ω_0 , s_1 and s_2 that set $\text{TE}_3 = 0$ and $\text{TE}_4 = 0$ as function of ϵ when $u/c = 0.1$, i.e. $\text{Pe}_{\Delta x} = 0.1/\epsilon$. The behaviour of the obtained curves is much smoother for the MRT-CM, see Fig. 2(a), than it is for the MRT-RM model, see Fig. 2(b). This may be attributed to the fact that, in the former, the structure of the TE_3 and TE_4 terms is much simpler. We note that a similar plotting analysis was presented for the MRT-RM model in [61]; check Fig. 1 of the Ref. [61]. Although the plot in [61] differs slightly from our Fig. 2(b), we believe that differences are due to the solution of Eqs. (39a) and (39b) having multiple roots. Concerning the subsets of the MRT model, i.e. the REG and BGK models, it is found that the BGK model requires fixating ϵ to reach the fourth-order accuracy, which reduces the curves to point solutions in Fig. 2(c). In practice, this means that it is not possible to improve the BGK accuracy and, at the same time, guarantee the physical regime to the desired Péclet number. Much more limited in this sense is the REG model that can never satisfy the condition leading to $\text{TE}_3 = 0$ and $\text{TE}_4 = 0$ and, consequently, can never reach fourth-order accuracy.

Fifth and last, after determining the ω_0 , s_1 and s_2 values that yield $\text{TE}_3 = 0$ and $\text{TE}_4 = 0$, for u/c and ϵ fixed, it is still required a stability proof [5] to guarantee that the LBM solutions are indeed fourth-order convergent. Section 6 presents the stability analysis of the LBM for the 1D ADE. Based on the analysis, which will be detailed in Section 6, we plot in Fig. 3 the stability domains over u/c and ϵ spaces, considering the ω_0 , s_1 and s_2 values that yield fourth-order accuracy, i.e. $\text{TE}_3 = 0$ and $\text{TE}_4 = 0$, for the MRT-CM, MRT-RM and BGK collision models. As expected the stability region narrows when u/c gets larger.¹ Contrary to expectations, for $u/c > 0.5$, the stability region supported by the MRT-CM model tends to be slightly smaller than that of the MRT-RM model. This narrowing in the stability domain of the MRT-CM model will become even more noticeable when repeating these tests for other ω_0 , s_1 and s_2 values, which do not set $\text{TE}_3 = 0$ and $\text{TE}_4 = 0$, like in the present case. Section 6 will provide more details on those stability maps.

¹ Stability also gets compromised in a thin strip around $\epsilon = 0$. Although it is hard to visualize in Fig. 3, this is the other situation where $\text{Pe}_{\Delta x} \gg 1$.

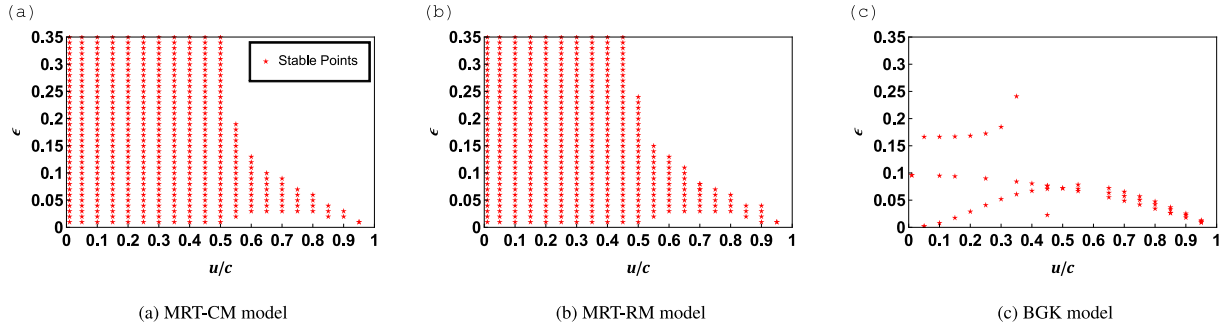


Fig. 3. Stability domain of the 4th order accurate solution. Note, grid Péclet number is defined by the ratio of the two axes, i.e. $Pe_{\Delta x} = \frac{u/c}{\epsilon} = \frac{u\Delta x}{D}$. Recall, $\epsilon = (1 - \omega_0)\Lambda_1$ and $D = \epsilon \Delta x^2 / \Delta t$.

6. Stability analysis of the EFD scheme

6.1. Stability of the MRT-CM model

This section derives the necessary and sufficient condition for the stability of the MRT-CM model for the 1D ADE, by studying its equivalent representation given by the FLFD scheme. As proven by Bellotti et al. [60], any LBM scheme may be rewritten as a corresponding multi-step FD scheme. In this way, the linear stability of the MRT-CM model, Eq. (2), can be proven by demonstrating the corresponding FLFD scheme, Eq. (25), is stable in the von Neumann sense. Such an equivalence permits focusing on the stability analysis of the FLFD scheme. Along these lines, we directly take the Fourier transform of the FLFD scheme described by Eq. (25), with coefficients represented by Eq. (26), so that the transformation $\hat{U}_j^{n+1} = \mathbf{H} \hat{U}_j^n$ takes the following amplification matrix [61]:

$$\mathbf{H} = \begin{bmatrix} \alpha_1 + \alpha_2 e^{-i\theta} + \alpha_3 e^{i\theta} & \beta_1 + \beta_2 e^{-i\theta} + \beta_3 e^{i\theta} & \gamma \\ 1 & 0 & 0 \\ 0 & 1 & 0 \end{bmatrix}$$

and the characteristic polynomial of \mathbf{H} can be written as:

$$p_3(\lambda) = \lambda^3 + a_2 \lambda^2 + a_1 \lambda + a_0 \quad (42)$$

with coefficients

$$a_2 = \left[-1 + s_2 \left(1 - \omega_0 + \frac{u^2}{c^2} \right) (1 - \cos \theta) - (2 - s_1 - s_2) \cos \theta + 2 \frac{u^2}{c^2} (s_1 - s_2) (1 - \cos \theta) \right] + i \left[\frac{u}{c} s_1 \sin \theta - 2 \frac{u}{c} (s_1 - s_2) \sin \theta \right] \quad (43a)$$

$$a_1 = \left[(1 - s_1) \left(1 - s_2 + s_2 \left(1 - \omega_0 + \frac{u^2}{c^2} \right) (1 - \cos \theta) \right) + (2 - s_1 - s_2) \cos \theta + 2 \frac{u^2}{c^2} (s_1 - s_2) (1 - \cos \theta) \right] + i \left[-\frac{u}{c} s_1 (1 - s_2) \sin \theta + 2 \frac{u}{c} (s_1 - s_2) \sin \theta \right] \quad (43b)$$

$$a_0 = (1 - s_1) (s_2 - 1) \quad (43c)$$

Remark 2. Once again, the underlined terms in this section represent the extra terms specific to the MRT-CM model, i.e. they signify the only difference between the MRT-CM and the MRT-RM discrete models.

It is noted that the linear stability of the MRT-RM model for the 1D ADE was already studied in [61,71] (although we note that in [61] the imaginary part of their a_2 and a_1 coefficients features opposite signs to ours, which however does not impact the end result as it is based on the absolute value of these coefficients). The purpose of this section is twofold: (i) to extend the stability analysis for the MRT-CM model and (ii) to compare the stability characteristics between the MRT-CM, MRT-RM, REG and BGK collision schemes for the 1D ADE problem considered in this work.

The procedure adopted to determine the stability criteria of the FLFD scheme is based on Miller's theorem [35]. This theorem provides the necessary and sufficient conditions to ensure that all roots of the characteristic polynomial in Eq. (42), denoted by λ_k ($k = 1, 2, 3$), fall inside or on the unit circle so that Eq. (42) is a von Neumann polynomial. According to Miller's theorem [35] if $|p_n^*(0)| - |p_n(0)| \geq 0$ (where $p_n^*(0)$ is defined ahead) then $p_n(\lambda)$ is a von Neumann polynomial when $p_{n-1}(\lambda)$ is a von Neumann polynomial. The determination of the conditions that ensure Eq. (42) is a von Neumann polynomial proceeds along the three steps detailed next [61].

Step 1.

Define the polynomials:

$$p_3^*(\lambda) = a_0 \lambda^3 + \bar{a}_1 \lambda^2 + \bar{a}_2 \lambda + 1 \quad (44a)$$

$$p_2(\lambda) = \frac{p_3^*(0)p_3(\lambda) - p_3(0)p_3^*(\lambda)}{(1 - a_0^2)\lambda^2 + (a_2 - a_0\bar{a}_1)\lambda + (a_1 - a_0\bar{a}_2)} \quad (44b)$$

where \bar{a}_i denotes the complex conjugate of a_i , and each coefficient above is expressed as follows:

$$\begin{aligned}
 1 - |a_0|^2 &= 1 - (1 - s_1)^2(1 - s_2)^2 \\
 a_2 - a_0\bar{a}_1 &= \left(1 - \omega_0 + \frac{u^2}{c^2}\right) s_2 (1 + (1 - s_1)^2(1 - s_2)) (1 - \cos \theta) \\
 &\quad - (2 - s_1 - s_2) (1 - (1 - s_1)(1 - s_2)) \cos \theta \\
 &\quad - (1 - (1 - s_1)^2(1 - s_2)^2) \\
 &\quad + 2(s_1 - s_2) (1 + (1 - s_1)(1 - s_2)) \left[\frac{u^2}{c^2} (1 - \cos \theta) - i \frac{u}{c} \sin \theta \right] \\
 &\quad + i \frac{u}{c} s_1 (1 + (1 - s_1)(1 - s_2)^2) \sin \theta \\
 a_1 - a_0\bar{a}_2 &= \left(1 - \omega_0 + \frac{u^2}{c^2}\right) s_2(1 - s_1)(2 - s_2)(1 - \cos \theta) \\
 &\quad + (2 - s_1 - s_2) (1 - (1 - s_1)(1 - s_2)) \cos \theta \\
 &\quad + 2(s_1 - s_2) (1 + (1 - s_1)(1 - s_2)) \left[\frac{u^2}{c^2} (1 - \cos \theta) + i \frac{u}{c} \sin \theta \right] \\
 &\quad - i \frac{u}{c} s_1(2 - s_1)(1 - s_2) \sin \theta
 \end{aligned} \tag{45}$$

To test if $p_3(\lambda)$ is a von Neumann polynomial, the following condition needs to be satisfied:

$$|p_3^*(0)| - |p_3(0)| \geq 0 \quad \Rightarrow \quad |1 - |a_0|| \geq 0 \quad \Leftrightarrow \quad 1 - (1 - s_1)^2(s_2 - 1)^2 \geq 0 \tag{46}$$

which is always true for $0 < s_1, s_2 < 2$. According to Theorem 6.1 in [60], the characteristic polynomial $p_3(\lambda)$, Eq. (42), is a von Neumann polynomial iff $p_2(\lambda)$, defined in Eq. (44b), is a von Neumann polynomial. The proof of this condition motivates the continuation of the recursive testing towards Step 2.

Step 2.

Define the polynomials:

$$p_2^*(\lambda) = (\bar{a}_1 - a_0a_2) \lambda^2 + (\bar{a}_2 - a_0a_1) \lambda + (1 - |a_0|^2) \tag{47a}$$

$$\begin{aligned}
 p_1(\lambda) &= \frac{p_2^*(0)p_2(\lambda) - p_2(0)p_2^*(\lambda)}{\lambda} \\
 &= [(1 - |a_0|^2)^2 - (a_1 - a_0\bar{a}_2)^2] \lambda + [(1 - |a_0|^2)(a_2 - a_0\bar{a}_1) - (a_1 - a_0\bar{a}_2)(\bar{a}_2 - a_0a_1)]
 \end{aligned} \tag{47b}$$

To test if $p_2(\lambda)$ is a von Neumann polynomial, the following condition needs to be satisfied:

$$|p_2^*(0)| - |p_2(0)| \geq 0 \quad \Rightarrow \quad |1 - |a_0|^2| - |a_1 - a_0\bar{a}_2| \geq 0 \tag{48}$$

Expanding Eq. (48), we obtain:

$$\begin{aligned}
 |1 - |a_0|^2| - |a_1 - a_0\bar{a}_2| &= \left|1 - (1 - s_1)^2(1 - s_2)^2\right| - \left| \left[\left(1 - \omega_0 + \frac{u^2}{c^2}\right) (1 - \cos \theta) + \cos \theta \right] s_2(1 - s_1)(2 - s_2) \right. \\
 &\quad \left. + s_1(1 - s_2)(2 - s_1) \left[\cos \theta - i \frac{u}{c} \sin \theta \right] \right. \\
 &\quad \left. + 2 \frac{u}{c} (s_1 - s_2) (1 + (1 - s_1)(1 - s_2)) \left[\frac{u}{c} (1 - \cos \theta) + i \sin \theta \right] \right| \geq 0
 \end{aligned} \tag{49}$$

Eq. (49) can be further developed with respect to the absolute values ($\times - 1$) and written in compact form as follows:

$$\begin{aligned}
 \max_{\theta \in [-\pi, \pi]} \left\{ \frac{u^2}{c^2} (1 - \cos^2 \theta) \Omega_{s_1}^2 + (\mathcal{A} (1 - \cos \theta) \Omega_{s_2} + \Gamma \cos \theta)^2 - \Omega^2 \right. \\
 \left. + 4 \frac{u^2}{c^2} \Theta (1 - \cos \theta) \left[2 \frac{u^2}{c^2} \Theta - \frac{u}{c} (1 + \cos \theta) \Omega_{s_1} + (\mathcal{A} (1 - \cos \theta) \Omega_{s_2} + \Gamma \cos \theta) \right] \right\} \leq 0
 \end{aligned} \tag{50}$$

where the parameters $\mathcal{A}, \Omega, \Omega_{s_1}, \Omega_{s_2}$ and Θ are defined ahead in Eq. (60).

While Eq. (50) may undergo variations within the $\theta \in [-\pi, \pi]$ interval, it is interesting to investigate the limit $\theta = \pi$, which corresponds to the necessary diffusion dominant condition [71]. We recall that, for the MRT-RM model to satisfy this condition, one must have $0 \leq \mathcal{A} \leq 1$, which translates to $\omega_0 \geq \frac{u^2}{c^2}$. At the same time, recall that the CFL condition enforces $0 \leq \frac{u}{c} \leq 1$. Then, the simultaneous fulfilment of these two conditions allows us to estimate the majorant of Eq. (49) given as follows:

$$\begin{aligned}
 \Omega^2 - \left[(\Omega_{s_1} - \Omega_{s_2}) - 4\Theta \right]^2 &\geq 0 \quad \Rightarrow \\
 \underbrace{(1 + (1 - s_1)(1 - s_2))^2}_{>0} \left((1 - (1 - s_1)(1 - s_2))^2 - 9(s_1 - s_2)^2 \right) &\geq 0 \quad \Rightarrow \\
 (1 - (1 - s_1)(1 - s_2))^2 - 9(s_1 - s_2)^2 &\geq 0
 \end{aligned} \tag{51}$$

The solution of the inequality in Eq. (51), under $0 < s_1, s_2 < 2$, is given by:

$$0 < s_1 < 2 \quad \text{and} \quad \frac{2s_1}{4 - s_1} \leq s_2 \leq \frac{4s_1}{2 + s_1}. \tag{52}$$

Fig. 4 plots the (s_2, s_1) stability domain determined by Eq. (52). As shown in this plot, the MRT-CM model is only stable inside the narrow strip around the $s_2 = s_1$ line with boundaries dictated by Eq. (52). It is worthwhile noticing that the upper limit, $s_2 = \frac{4s_1}{2+s_1}$, is the relaxation combination that cancels the u^2 -artefact on the coefficient D_{eff} of the MRT-CM model for the steady-state ADE, derived in Section 4.

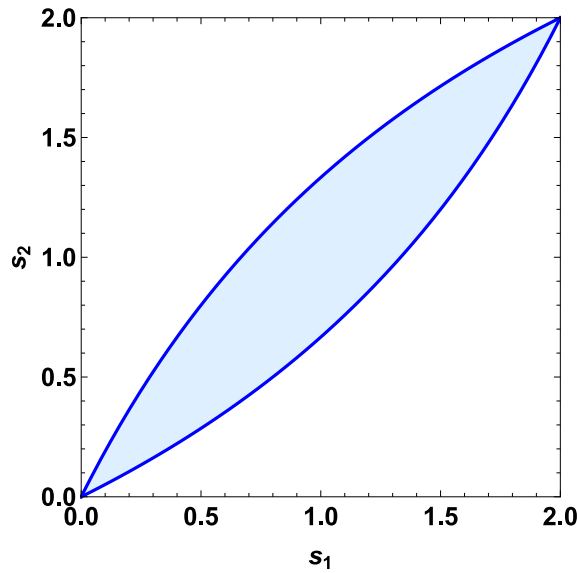


Fig. 4. Shaded area denotes the stability region in the (s_2, s_1) domain according to Eq. (52), which is a prediction for the majorant of Eq. (50).

Finally, the polynomial $p_2(\lambda)$, Eq. (44b), is a von Neumann polynomial iff $p_1(\lambda)$, defined in Eq. (53b), is a von Neumann polynomial, which will be evaluated on Step 3.

Step 3.

Define the polynomials:

$$p_1(\lambda) = [(1 - |a_0|^2)^2 - (a_1 - a_0\bar{a}_2)^2] \lambda + [(1 - |a_0|^2)(a_2 - a_0\bar{a}_1) - (a_1 - a_0\bar{a}_2)(\bar{a}_2 - a_0a_1)] \tag{53a}$$

$$p_1^*(\lambda) = [(1 - |a_0|^2)(a_2 - a_0\bar{a}_1) - (a_1 - a_0\bar{a}_2)(\bar{a}_2 - a_0a_1)] \lambda + [(1 - |a_0|^2)^2 - (a_1 - a_0\bar{a}_2)^2] \tag{53b}$$

To test if $p_1(\lambda)$ is a von Neumann polynomial, the following condition needs to be satisfied:

$$|p_1^*(0)|^2 - |p_1(0)|^2 \geq 0 \Rightarrow \left| (1 - |a_0|^2)^2 - (a_1 - a_0\bar{a}_2)^2 \right|^2 - \left| (1 - |a_0|^2)(a_2 - a_0\bar{a}_1) - (a_1 - a_0\bar{a}_2)(\bar{a}_2 - a_0a_1) \right|^2 \geq 0 \tag{54}$$

To facilitate the analysis, we follow [61] and split the real and imaginary parts of those complex numbers as follows:

$$\begin{aligned} 1 - |a_0|^2 &= a_r \\ a_2 - a_0\bar{a}_1 &= a_{r11} + i a_{r12} \\ a_1 - a_0\bar{a}_2 &= a_{r21} + i a_{r22} \\ \bar{a}_2 - a_0a_1 &= a_{r11} - i a_{r12} \end{aligned} \tag{55}$$

where

$$\begin{aligned} a_r &= \Omega \\ a_{r11} &= \mathcal{A} (1 - \cos \theta) \Gamma_{s_1} - \Gamma \cos \theta - \Omega + 2 \frac{u^2}{c^2} \Theta (1 - \cos \theta) \\ a_{r12} &= \frac{u}{c} \Gamma_{s_2} \sin \theta - 2 \frac{u}{c} \Theta \sin \theta \\ a_{r21} &= \mathcal{A} (1 - \cos \theta) \Omega_{s_2} + \Gamma \cos \theta + 2 \frac{u^2}{c^2} \Theta (1 - \cos \theta) \\ a_{r22} &= -\frac{u}{c} \Omega_{s_1} \sin \theta + 2 \frac{u}{c} \Theta \sin \theta. \end{aligned} \tag{56}$$

The parameters introduced above, i.e. \mathcal{A} , Ω , Ω_{s_1} , Ω_{s_2} , Γ_{s_1} , Γ_{s_2} and Θ , are defined in Eq. (60). The inclusion of Eq. (55) into Eq. (54) ($\times - 1$) yields:

$$|a_r(a_{r11} + i a_{r12}) - (a_{r21} + i a_{r22})(a_{r11} - i a_{r12})| + |a_{r21} + i a_{r22}|^2 - |a_r|^2 \leq 0 \tag{57}$$

The simplification of Eq. (57) reads:

$$(a_r a_{r11} - a_{r21} a_{r11} - a_{r22} a_{r12})^2 + (a_r a_{r12} + a_{r21} a_{r12} - a_{r22} a_{r11})^2 - (a_r^2 - a_{r21}^2 - a_{r22}^2)^2 \leq 0 \tag{58}$$

After a few algebraic manipulations, Eq. (58) can be recast as follows:

$$\begin{aligned}
 \max_{\theta \in [-\pi, \pi]} \left\{ \frac{u^4}{c^4} (1 - \cos^2 \theta)^2 \Omega_{s_1}^2 (\Omega - \Gamma) (\Gamma_{s_2} + \Omega_{s_1}) \right. \\
 + \frac{u^2}{c^2} (1 - \cos^2 \theta) \left[\mathcal{A}^2 (1 - \cos \theta)^2 (\Omega - \Gamma) \left[\Omega_{s_1}^2 (\Gamma_{s_1} + \Omega_{s_2}) + \Omega_{s_2}^2 (\Gamma_{s_2} + \Omega_{s_1}) \right] \right. \\
 + \mathcal{A} (1 - \cos \theta) 2 \Omega \left[\Gamma_{s_1} \Omega_{s_1} (\Omega - \Gamma) + \Gamma_{s_2} (\Gamma_{s_1} \Omega_{s_1} + \Gamma_{s_2} \Omega_{s_2}) \right] \\
 + \Omega^2 (\Omega - \Gamma) (\Gamma_{s_2} - 3 \Omega_{s_1}) \left. \right] \\
 + \mathcal{A} (1 - \cos \theta) (\Gamma_{s_1} + \Omega_{s_2}) \left[(-\mathcal{A}^2 (1 - \cos \theta)^2 2 \Gamma_{s_1} \Omega_{s_2} + \mathcal{A} (1 - \cos \theta) \Omega (\Gamma_{s_1} + 3 \Omega_{s_2}) - 2 \Omega^2) \Omega \right. \\
 + (\mathcal{A}^2 (1 - \cos \theta)^2 \Omega_2 (\Gamma_{s_1} - 2 \Omega_{s_2}) - \mathcal{A} (1 - \cos \theta) \Omega (\Omega - \Gamma) + \Omega^2) 2 \Gamma \cos \theta \\
 + (\mathcal{A} (1 - \cos \theta) (\Gamma_{s_1} - 5 \Omega_{s_2}) + 2 \Omega) \Gamma^2 \cos^2 \theta \\
 \left. - \mathcal{A}^2 (1 - \cos \theta)^2 2 \Gamma^3 \cos^3 \theta \right] \\
 \left. + \frac{u^6}{c^6} \Phi_6 + \frac{u^4}{c^4} \Phi_4 + \frac{u^2}{c^2} \Phi_2 \right\} \leq 0
 \end{aligned} \tag{59}$$

with

$$\begin{aligned}
 \mathcal{A} &= 1 - \omega_0 + \frac{u^2}{c^2} \\
 \Omega &= 1 - (1 - s_1)^2 (1 - s_2)^2 \\
 \Omega_{s_1} &= s_1 (2 - s_1) (1 - s_2) \quad \Omega_{s_2} = s_2 (2 - s_2) (1 - s_1) \\
 \Gamma &= \Omega_{s_1} + \Omega_{s_2} \\
 \Gamma_{s_1} &= \Omega - \Omega_{s_1} \quad \Gamma_{s_2} = \Omega - \Omega_{s_2} \\
 \Theta &= (s_1 - s_2) (1 + (1 - s_1) (1 - s_2))
 \end{aligned} \tag{60}$$

where in detail we have

$$\begin{aligned}
 \Gamma &= \Omega_{s_1} + \Omega_{s_2} = (2 - s_1 - s_2) (1 - (1 - s_1) (1 - s_2)) = s_1 (2 - s_1) (1 - s_2) + s_2 (1 - s_1) (2 - s_2) \\
 \Gamma_{s_1} &= \Omega - \Omega_{s_1} = s_2 (1 + (1 - s_1)^2 (1 - s_2)) = (1 - (1 - s_1)^2 (1 - s_2)^2) - s_1 (2 - s_1) (1 - s_2) \\
 \Gamma_{s_2} &= \Omega - \Omega_{s_2} = s_1 (1 + (1 - s_1) (1 - s_2)^2) = (1 - (1 - s_1)^2 (1 - s_2)^2) - s_2 (1 - s_1) (2 - s_2)
 \end{aligned}$$

and the terms specific to the MRT-CM model, Φ_6 , Φ_4 and Φ_2 , are explicitly given as follows:

$$\begin{aligned}
 \Phi_6 &= -16 \Theta^3 (1 - \cos \theta)^3 [\mathcal{A} (1 - \cos \theta) (\Gamma - \Omega) - 2 (\Gamma - \Omega) + (\Gamma + \Omega) (1 + \cos \theta)] \\
 &\quad - 4 \Theta^2 (1 - \cos \theta)^2 (\Gamma - \Omega) (\Gamma_{s_2} + \Omega_{s_1}) (1 - \cos^2 \theta)
 \end{aligned} \tag{61}$$

$$\begin{aligned}
 \Phi_4 &= -16 \Theta^3 (1 - \cos \theta)^3 (1 + \cos \theta) [\mathcal{A} (\Gamma - \Omega) - (\Gamma + \Omega)] \\
 &\quad + \Theta^2 (1 - \cos \theta)^2 \left[4 \mathcal{A}^2 (1 - \cos \theta)^2 (\Omega - \Gamma) (\Omega - \Gamma + 6 \Omega \Omega_{s_2}) \right. \\
 &\quad \quad - 8 \mathcal{A} (1 - \cos \theta) ((\Omega - \Gamma) (3 \Omega + 2 \Gamma) + 6 \Omega \Omega_{s_2}) \\
 &\quad \quad + 2 (\Gamma + 3 \Omega + 10 \Omega_{s_1}) (\Omega - \Gamma) + 16 \Omega \Omega_{s_2} \\
 &\quad \quad - 8 [\mathcal{A} (1 - \cos \theta) \Gamma (\Omega - \Gamma + 6 \Omega_{s_2}) \\
 &\quad \quad \quad + (3 \Omega - \Gamma) (\Omega + \Gamma) - 2 (\Omega \Gamma + \Omega \Omega_{s_1} + \Gamma \Omega_{s_2}) \left. \right] \cos \theta \\
 &\quad + 2 [(\Omega^2 - \Gamma^2) - 2 \Omega_{s_2} (3 \Omega + \Gamma)] \cos(2\theta) \\
 &\quad + 4 \Theta (1 - \cos \theta) (1 - \cos^2 \theta) \left[\mathcal{A} (1 - \cos \theta) \left[(\Omega - \Gamma) \Omega_{s_1}^2 - \Omega_{s_2} \left(\Omega_{s_1}^2 - (\Omega - \Omega_{s_2})^2 \right) \right] \right. \\
 &\quad \quad - (\Omega - \Omega_{s_1}) \left[(\Omega - \Gamma)^2 - 2 (\Omega - \Omega_{s_2})^2 \right] - \Omega_{s_1}^2 (\Omega + \Omega_{s_1} - \Omega_{s_2}) \\
 &\quad \quad - [\Omega_{s_1} (\Omega - \Gamma) (\Omega - \Gamma + 3 \Omega_{s_1}) \\
 &\quad \quad \quad - \Gamma (\Gamma^2 + \Omega^2 - \Omega_{s_2} (2 \Omega + \Omega_{s_1}) - \Omega_{s_1} (\Gamma + 3 \Omega_{s_1})) \left. \right] \cos \theta
 \end{aligned} \tag{62}$$

$$\begin{aligned}
\Phi_2 = & 4 \Theta^2 (1 - \cos \theta)^2 \left[\mathcal{A}^2 (1 - \cos^2 \theta) (\Omega - \Gamma) (\Gamma_{s_1} + \Omega_{s_2}) \right. \\
& \left. + 2 \mathcal{A} (1 + \cos \theta) (\Omega - \Gamma \cos \theta) (\Gamma_{s_1} + \Omega_{s_2}) \right] \\
& + \Theta (1 - \cos \theta) \left[4 \mathcal{A}^3 (1 - \cos \theta)^3 \Omega_{s_2} (\Omega - \Gamma) (2 \Omega_{s_2} + \Gamma_{s_1}) \right. \\
& - 4 \mathcal{A}^2 (1 - \cos \theta)^2 \left[(\Gamma_{s_1}^2 + \Omega_{s_2}^2) (\Omega + \Omega_{s_1}) + 4 \Gamma_{s_1} \Omega_{s_2} \Omega + \Omega_{s_2}^2 (\Omega - \Gamma - 2 \Omega_{s_1}) \right. \\
& \quad \left. \left. + \left((\Gamma_{s_1}^2 - \Omega_{s_2}^2) (\Omega_{s_1} - \Gamma) + \Omega_{s_2}^2 (\Omega + 5 \Gamma) \right) \cos \theta \right] \right. \\
& + 2 \mathcal{A} (1 - \cos \theta) \left[(\Omega - \Omega_{s_1}) (2 \Omega^2 + 2 \Gamma \Omega_{s_1} - \Gamma^2) \right. \\
& \quad - \Omega_{s_2} (7 \Gamma^2 + 2 \Gamma (\Omega - 2 \Omega_{s_1}) + 2 \Omega (2 \Omega_{s_1} - 5 \Omega)) + 2 \Omega_{s_2}^2 (\Gamma + 2 \Omega) \\
& \quad - 4 (\Gamma_{s_2} \Omega (\Gamma_{s_1} + \Omega_{s_2}) + \Gamma \Gamma_{s_1} (\Omega - \Omega_{s_1}) - \Gamma \Omega_{s_2} (\Gamma + \Omega_{s_1})) \cos \theta \\
& \quad \left. - \Gamma (2 \Omega_{s_2} (\Gamma_{s_2} - 2 \Omega_{s_1}) + \Gamma (\Gamma_{s_1} + 7 \Omega_{s_2}) - 2 \Gamma_{s_1} \Omega_{s_1}) \cos(2\theta) \right] \\
& \left. + (\Omega + \Gamma) (2 (\Gamma^2 - 2 \Omega^2) - (3 \Gamma^2 - 4 \Omega^2) \cos \theta + 2 \Gamma^2 \cos(2\theta) + \Gamma^2 \cos(3\theta)) \right] \quad (63)
\end{aligned}$$

Conclusion. The MRT-CM as a numerical model for the 1D ADE is stable in the von Neumann sense iff it simultaneously satisfies the following five stability conditions: (i) $0 \leq \omega_0 \leq 1$, (ii) $0 \leq u/c \leq 1$, (iii) $\omega_0 \geq \frac{u^2}{c^2}$, (iv) Eq. (50), and (v) Eq. (59).

Among the five stability conditions, Eq. (59) is the more restrictive one. Focusing on Eq. (59), the only difference between the MRT-CM and MRT-RM comes from the extra terms Φ_6 , Φ_4 and Φ_2 , which scale with u^6/c^6 , u^4/c^4 and u^2/c^2 , respectively. Consequently, the larger is the u/c ratio, the more significant the impact of these terms becomes and, consequently, the larger the differences between MRT-CM and MRT-RM will be. This explains the differences between MRT-CM and MRT-RM stability plots shown in Fig. 3, which only become noticeable for $u/c > 0.5$ (a result that will be made more evident below). Since the ensemble of stability conditions obtained in this analysis leads to a highly non-linear problem, its analytical study poses a rather challenging endeavour. In alternative, our stability study will be based on the numerical solution of the aforementioned set of inequalities.

Figs. 5, 6, 7 and 8 display the stability maps obtained numerically, over the parameter space of u/c and ω_0 equilibrium terms, for the MRT-CM and MRT-RM models, where for each panel it is illustrated the effect of increasing Λ_1 holding Λ , with $\Lambda = 1/20$, $\Lambda = 1/12$, $\Lambda = 1/4$ and $\Lambda = 1/2$ fixed, respectively. Overall, these plots provide a general picture on the stability domains of MRT-CM and MRT-RM models, and allows us to withdraw the following conclusions.

On the one hand, below $u/c = 0.5$, the stability domain of the MRT-CM model is typically broader than the MRT-RM. Particularly, MRT-CM remains stable at smaller $1 - \omega_0$ values. That is, in the $u/c \leq 0.5$ range, the MRT-CM is able to reach higher grid Péclet values, $Pe_{\Delta x} = \frac{u/c}{\epsilon}$, because it is able to support smaller $1 - \omega_0$ values or, equivalently, it is able to support smaller viscosities $\epsilon = (1 - \omega_0) \Lambda_1$ for a given Λ_1 relaxation coefficient. Yet, this trend changes for relatively high values of Λ_1 or Λ , where MRT-RM becomes the stabler scheme in the subinterval $u/c \leq 0.5$.

On the other hand, above $u/c = 0.5$, the stability domain of the MRT-CM model falls rapidly towards an empty set. This behaviour is only avoided for Λ_1 (hence, viscosity) being made large. In this case, reaching high grid Péclet number in the $u/c \geq 0.5$ subinterval is very challenging as it demands the use of large viscosities (hence, bringing $Pe_{\Delta x} = \frac{u/c}{\epsilon}$ down). Consequently, when operating at $u/c \geq 0.5$ over the typical range of relaxation parameters, it is safer to use the MRT-RM scheme.

From a practical perspective, the stability study here presented provides three main messages. First, the unique adoption of the comoving frame in the LBM collision model may deteriorate the stability support of the LBM solution; an observation in line with the numerical study of Dubois and Février [13], which indicated that the inclusion of an extended equilibrium² is crucial for the stability of the MRT-CM model. Second, the Φ_6 , Φ_4 and Φ_2 extra terms, which are specific to the MRT-CM model, and scale with u^6/c^6 , u^4/c^4 and u^2/c^2 , respectively, may lead to opposing effects. When u/c is moderately small (providing ϵ is small too), those terms may help stabilizing the MRT-CM solution. When u/c increases, they quickly tend to dominate the stability condition and cause the MRT-CM solution to abruptly blow up. Third, the MRT-CM is also far more susceptible to the individual values of the relaxation rates, s_1 and s_2 , particularly, when they become too dissimilar, as illustrated in Fig. 4. For example, the attempt to enhance stability by reducing the grid Péclet, $Pe_{\Delta x}$, through the increase of s_1 is only effective if the other relaxation rate s_2 is varied accordingly. Another example on the sensitivity of the MRT-CM stability towards the individual relaxation rates is the lack of an optimal stability condition for this collision operator. This point will be discussed in the next section.

6.2. Revisiting the optimal stability condition of the MRT-RM model [45,71,73]

Looking at Figs. 7 and 8 that refer to $\Lambda = 1/4$ and $\Lambda = 1/2$, respectively, it is noted that the stability maps of the MRT-RM are almost identical. Taking into account that the choice $\Lambda = 1/4$ has been coined as the ‘‘optimal stability condition’’ [45,71,73] for the TRT scheme (which is identical to the MRT-RM in the D1Q3 lattice), this observation might be surprising as the $\Lambda = 1/4$ case is often (erroneously) expected to support the larger stability domain among all Λ values. Here, we would like to take the opportunity to clarify this misunderstanding (which we note that it has been originally explained in the papers of Ginzburg and coworkers [45,71,73], but it continues being misinterpreted).

Following [45,71,73], the optimal stability condition is set by $\Lambda = \left(\frac{1}{s_1} - \frac{1}{2}\right) \left(\frac{1}{s_2} - \frac{1}{2}\right) = \frac{1}{4}$ or equivalently by $s_2 = 2 - s_1$. Dropping the underlined terms in Eq. (42), so that we retrieve the MRT-RM formulation, then the characteristic polynomial given by Eq. (42), with $s_2 = 2 - s_1$, can be expressed in factorized form as follows:

$$p_3(\lambda) = (1 - s_1 + \lambda) \left[\lambda^2 + \lambda \left[(s_1 - 2) \left(1 - \left(1 - \omega_0 + \frac{u^2}{c^2} \right) (1 - \cos \theta) \right) + i s_1 \frac{u}{c} \sin \theta \right] + (1 - s_1) \right]. \quad (64)$$

² In the D1Q3 lattice model, no expansion beyond the second order is possible for the equilibrium, meaning that an extended equilibrium is unavailable [7]. The support of an extended equilibrium in 1D is only possible with higher order velocity discretizations, such as D1Q5 or D1Q7 [72].

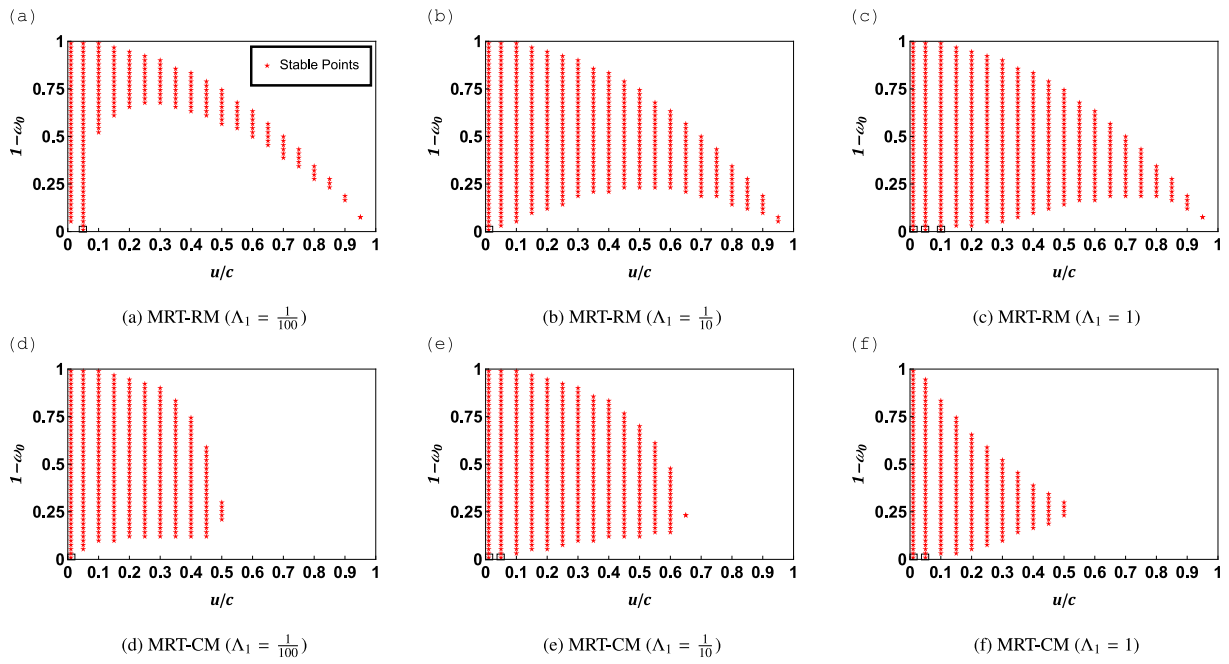


Fig. 5. Stability domains of MRT-RM and MRT-CM schemes fixing $\Lambda = 1/20$. Recall, $(1 - \omega_0) = \epsilon/\Lambda_1$.

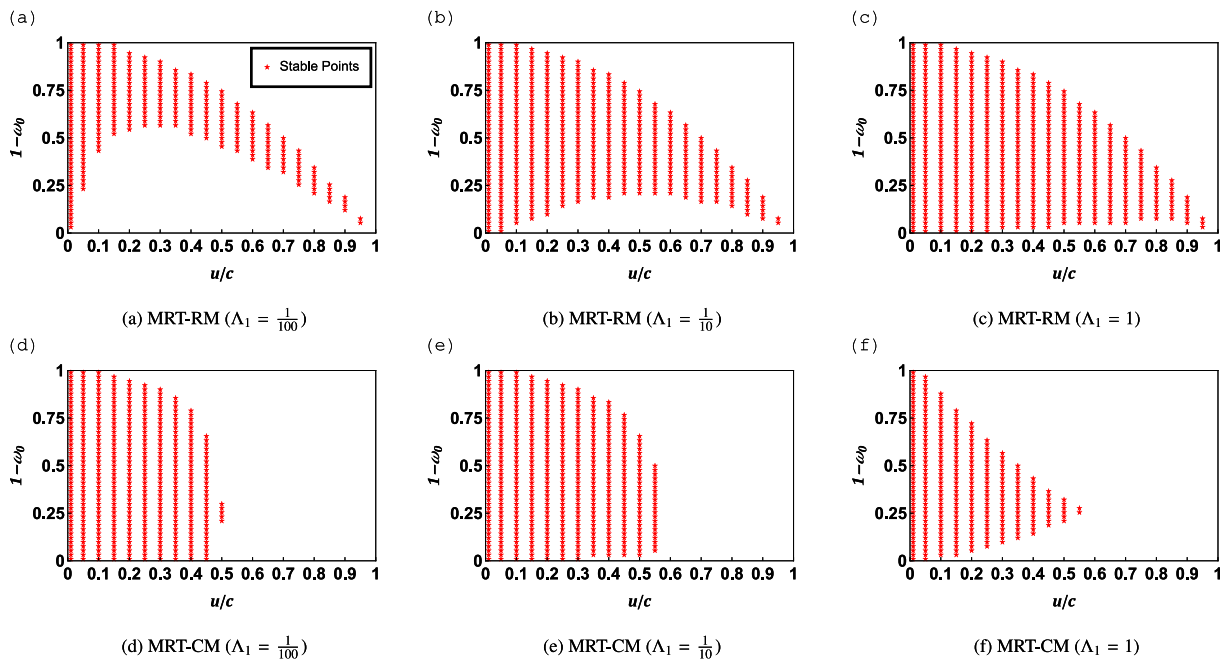


Fig. 6. Stability domains of MRT-RM and MRT-CM schemes fixing $\Lambda = 1/12$. Recall, $(1 - \omega_0) = \epsilon/\Lambda_1$.

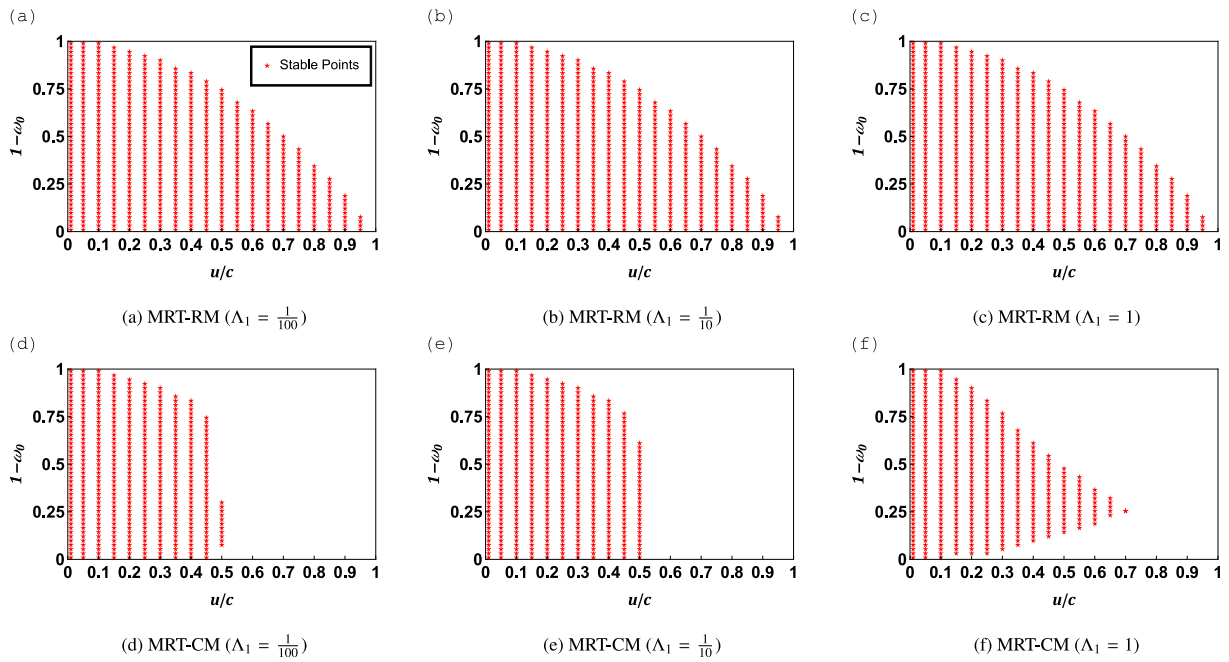


Fig. 7. Stability domains of MRT-RM and MRT-CM schemes fixing $\Lambda = 1/4$. Recall, $(1 - \omega_0) = \epsilon/\Lambda_1$.

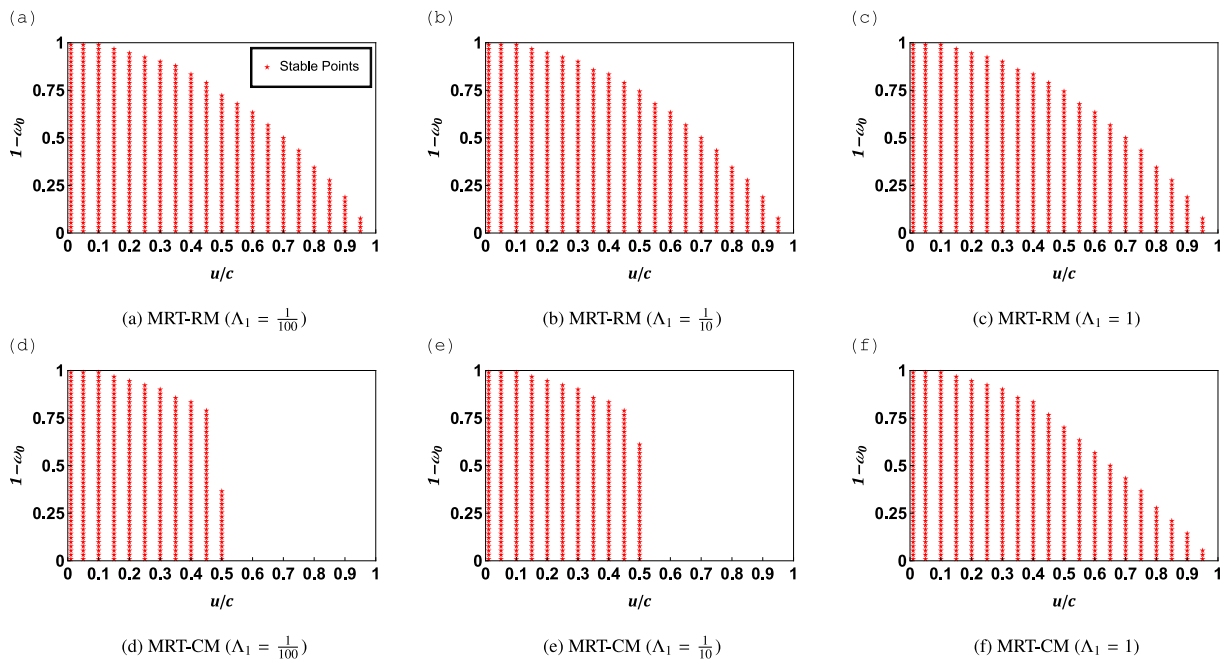


Fig. 8. Stability domains of MRT-RM and MRT-CM schemes fixing $\Lambda = 1/2$. Recall, $(1 - \omega_0) = \epsilon/\Lambda_1$.

According to Eq. (64), the roots of $p_3(\lambda)$ may be given by the very restrictive condition $s_1 = 1$, a case that boils down to the BGK setting $s_1 = s_2 = s = 1$, or otherwise by the more general condition set by the solution of the quadratic equation:

$$p_2(\lambda) = \lambda^2 + \lambda \left[(s_1 - 2) \left(1 - \left(1 - \omega_0 + \frac{u^2}{c^2} \right) (1 - \cos \theta) \right) + i s_1 \frac{u}{c} \sin \theta \right] + (1 - s_1). \quad (65)$$

The necessary and sufficient stability conditions of the MRT-RM model with $\Lambda = 1/4$ can be determined by the roots of $p_2(\lambda)$, which will be analysed next by applying Miller's theorem [35].

Step 1.

To test if $p_2(\lambda)$ is a von Neumann polynomial it needs to verify $|p_2(0)| < |p_2^*(0)|$, which is equivalent to $|1 - s_1| < 1$ and is always valid for $0 < s_1 < 2$.

Step 2.

Define the polynomial $p_1(\lambda) = \frac{p_2^*(0)p_2(\lambda) - p_2(0)p_2^*(\lambda)}{\lambda}$, which after a few manipulations can be factorized as follows:

$$p_1(\lambda) = (1 - (1 - s_1)^2) \left[\lambda - \underbrace{\left(1 - \left(1 - \omega_0 + \frac{u^2}{c^2} \right) (1 - \cos \theta) \right)}_{=C_1} + i \underbrace{\frac{u}{c} \sin \theta}_{=C_2} \right] = (1 - (1 - s_1)^2) \left[\lambda - (C_1 - i C_2) \right]. \quad (66)$$

Considering that the prefactor $(1 - (1 - s_1)^2) < 1$ for $0 < s_1 < 2$, then it follows that the stability of $p_1(\lambda)$ under $|\lambda|^2 \leq 1$ is determined by the condition $C_1^2 + C_2^2 \leq 1$. That is, the distinctive feature of the ‘‘optimal stability condition’’ is not that it offers a ‘‘better stability’’, but the fact that, with the specific relaxation combination $\Lambda = 1/4$, the stability behaviour of the LBM time-dependent solution becomes completely independent from the individual relaxation rates values, s_1 and s_2 , and only determined by the equilibrium parameters ω_0 and u/c , as shown in Eq. (66) and visible in Fig. 7(a), (b) and (c).

Remark 3. To finalize this section, we note that the extension of the above analysis to the MRT-CM model reveals that the formulation of MRT in the comoving frame does not support a similar kind of ‘‘optimal stability condition’’, meaning that there is no specific relaxation combination Λ that guarantees the model stability characteristics to be independent of the individual relaxation rates s_1 and s_2 , and only be controlled by the equilibrium parameters ω_0 and u/c .

7. Numerical tests

This section presents the numerical verification of the theoretical results previously reported. To this end, we will consider 1D time-dependent ADE problems governed by the two non-dimensional physical groups:

- (1) Péclet number: $Pe = \frac{uL}{D}$,
- (2) Fourier number: $Fo = \frac{tD}{L^2} = \bar{t}$.

The FLFD scheme implementation of the different LBM collision operators is employed. In this framework, the initial condition employs the known analytical solution at the first three time levels. Then, the time-dependent solution is let evolve until the desired \bar{t} value is reached. In terms of the computational performance, among tested collision schemes, the following relationship MRT-CM > MRT-RM > BGK is noted. That is, compared to the BGK model, the MRT-RM employs more operations every time step, due to the shift between moments and populations spaces, and this number gets augmented with the inclusion of the velocities in the transformation matrices, which makes the MRT-CM model the most computationally demanding. The REG model was not tested here as it does not support the intended 4th order accuracy.

In what follows, the accuracy of numerical solutions will be determined by the L_2 measure, which is defined as:

$$L_2(\phi) = \sqrt{\sum_j (\phi_j^n - \phi_j^{n(\text{analy})})^2 / \sum_j (\phi_j^{n(\text{analy})})^2} \quad (67)$$

where sums are taken over the full computational domain at time level n , determined as $n = \bar{t} \times L^2 / (D \Delta t) = \bar{t} \times N_x^2 / \epsilon$ where $L = N_x \Delta x$.

7.1. Advection-diffusion evolution of a Gaussian hill

Consider the transport of a Gaussian hill pulse, which is described by the following analytical solution [3,68]:

$$\bar{\phi}(\bar{x}, \bar{t}) = \frac{(2\pi \bar{\sigma}_0^2)^{d/2}}{(2\pi(\bar{\sigma}_0^2 + 2\bar{t}))^{d/2}} \exp \left[-\frac{(\bar{x} - \bar{x}_0 - Pe \bar{t})^2}{2(\bar{\sigma}_0^2 + 2\bar{t})} \right], \quad (68)$$

where d refers to the space dimension (here $d = 1$). The pulse non-dimensional solution is $\bar{\phi} = \phi/\phi_0$. In this work, we consider the initial pulse magnitude $\phi_0 = 1$ (simulation units), the initial pulse location $\bar{x}_0 = x_0/L = \frac{1}{2}$ and the initial pulse width $\bar{\sigma}_0 = \sigma_0/L = 0.05$ (both in non-dimensional scales). The non-dimensional spatial domain coordinate is $\bar{x} = x/L \in [0, 1]$, with domain length L discretized as follows $L = N_x \Delta x$. Periodic boundary conditions are applied at both ends of the domain and the problem initial condition is given by Eq. (68) with $\bar{t} = 0$. Note that, for a given time evolution \bar{t} , the solution $\bar{\phi}$ is uniquely governed by Pe , which is set as follows $Pe = \frac{u/c}{\epsilon} N_x = \frac{u \Delta x N_x}{(1 - \omega_0) c^2 \Lambda_1 \Delta t} = \frac{uL}{D}$.

Fig. 9 illustrates the LBM solutions, over the different collision operators, employing the free parameters $\{\omega_0, \Lambda_1, \Lambda\}$ that lead to the 4th order accurate solution,³ against the analytical profile, given by Eq. (68), for $\bar{t} = 0.001$, $Pe = 1$ and $\epsilon = 0.1$. Other Pe numbers were tested revealing

³ For example, for $Pe = 1$ and $\epsilon = 0.1$ (with $N_x = 81$ grid points), the free parameters in the MRT-RM are set as $\omega_0 = 0.879999207439141$, $s_1 = 0.7500003095933185$, and $s_2 = 1.24999870822213$, and in the MRT-CM are set as $\omega_0 = 0.399999330375504$, $s_1 = 1.50000041851495$, and $s_2 = 0.999999441979898$. The value of these parameters varies slightly with grid resolution N_x , when ϵ and Pe are fixed, but highly depends on Pe .

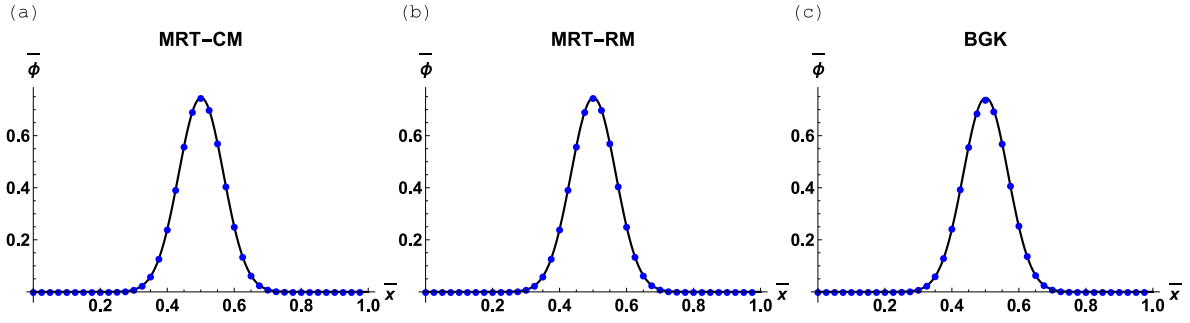


Fig. 9. Gaussian hill pulse solution profile for $Pe = 1$ and $\epsilon = 0.1$ at $\bar{t} = 0.001$ using $N_x = 41$, with free parameters $\{\omega_0, \Lambda_1, \Lambda\}$ leading to $TE_3 = 0$ and $TE_4 = 0$ according to Section 5. Black continuous line denotes the analytical solution [Eq. (68)]. Circles denote the numerical solution. Panel (a): MRT-CM ($L_2 = 6.08 \times 10^{-5}$). Panel (b): MRT-RM ($L_2 = 6.28 \times 10^{-5}$). Panel (c): BGK ($L_2 = 4.11 \times 10^{-3}$ and $Pe = 1.03984 \neq 1$ in this case).

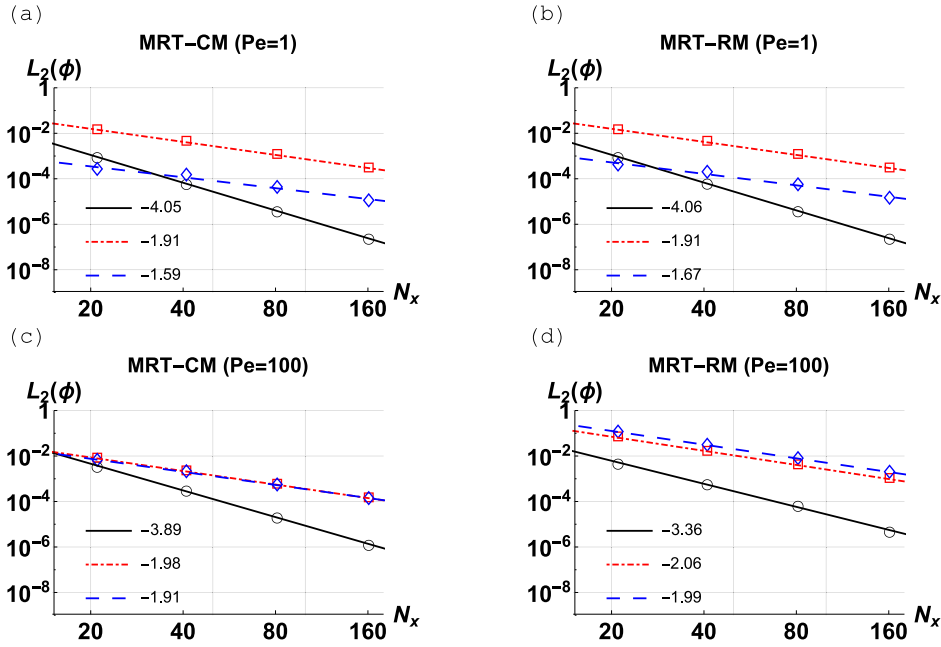


Fig. 10. Mesh convergence solutions of the Gaussian hill pulse problem for $\bar{t} = 0.001$. Symbols: circles (black) use the free parameters $\{\omega_0, \Lambda_1, \Lambda\}$ that lead to $TE_3 = 0$ and $TE_4 = 0$, diamonds (blue) use $\omega_0 = 2/3$ and $\Lambda = 1/6$, and squares (red) use $\omega_0 = 2/3$ and $\Lambda = 1/12$. Insets quantify the converge rates given by the slopes of fitting lines obtained from linear regression. Panel (a): MRT-CM for $Pe = 1$ and $\epsilon = 0.1$. Panel (b): MRT-RM for $Pe = 1$ and $\epsilon = 0.1$. Panel (c): MRT-CM for $Pe = 100$ and $\epsilon = 0.01$. Panel (d): MRT-RM for $Pe = 100$ and $\epsilon = 0.01$.

that the higher is Pe the larger will be the shift in the pulse peak from its origin $\bar{x}_0 = \frac{1}{2}$. We note that, for a fixed Pe number, both MRT-CM and MRT-RM collision models are able to adjust the free parameters $\{\omega_0, \Lambda_1, \Lambda\}$ so that 4th order accurate solutions can be retrieved. This contrasts with the BGK collision model, which only offers $\{\omega_0, \Lambda_1\}$ as free parameters, which precludes the simultaneous fulfilment of the 4th order accurate condition and the intended Pe number. In other words, given the grid resolution N_x and the Pe number, determined by $Pe = \frac{u/c}{\epsilon} N_x = \frac{u \Delta x N_x}{(1-\omega_0)c^2 \Lambda_1 \Delta t}$, it is generally not possible for the LBM-BGK model to meet the 4th order accurate condition for $\{\omega_0, \Lambda_1\}$ that guarantees $TE_3^{BGK} = 0$ and $TE_4^{BGK} = 0$ according to Eqs. (41a) and (41b), respectively.

Fig. 10 depicts the evolution of the LBM numerical error for the MRT-CM and MRT-RM models at a given Pe as function of the N_x mesh resolution. The BGK model is not considered in this analysis as it cannot simultaneously fulfil the 4th order accurate condition and the intended Pe number while varying N_x . The numerical solutions in Fig. 10 confirm the theoretical results presented in Section 5. That is, the proper choice of the free parameters $\{\omega_0, \Lambda_1, \Lambda\}$ that yield $TE_3 = 0$ and $TE_4 = 0$ leads to approximately a 4th order mesh convergence rate. Although, at large Pe values, the convergence rate is slightly deteriorated, it gets more affected in the MRT-RM model than in the MRT-CM model. For comparison purposes, other free parameter choices were also tested, by using $\omega_0 = 2/3$ and either $\Lambda = 1/12$ (optimal advection condition for steady-state equations) or $\Lambda = 1/6$ (optimal diffusion condition for steady-state equations). As expected, based on the LBM accuracy analysis developed in Section 5, the obtained LBM solutions follow a second order convergence rate towards the 1D time-dependent ADE solution, except when $TE_3 = 0$ and $TE_4 = 0$ are verified.

7.2. Advection–diffusion evolution of a time-decaying wave

Consider the transport of the exponentially decaying wave, which is described by the following analytical solution [61]:

$$\bar{\phi}(\bar{x}, \bar{t}) = \sin[k_x(\bar{x} - \bar{x}_0 - Pe\bar{t})] \exp[-k_x^2 \bar{t}] \quad (69)$$

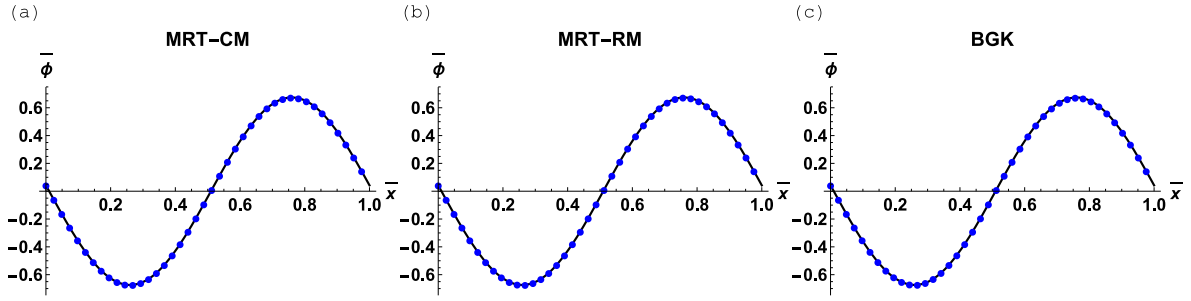


Fig. 11. Time-decaying wave solution profile for $Pe = 1$ and $\epsilon = 0.1$ at $\bar{t} = 0.01$ using $N_x = 41$, with free parameters $\{\omega_0, \Lambda_1, \Lambda\}$ leading to $TE_3 = 0$ and $TE_4 = 0$ according to Section 5. Black continuous line denotes the analytical solution [Eq. (69)]. Circles denote the numerical solution. Panel (a): MRT-CM ($L_2 = 2.66 \times 10^{-7}$). Panel (b): MRT-RM ($L_2 = 2.66 \times 10^{-7}$). Panel (c): BGK ($L_2 = 5.13 \times 10^{-4}$ and $Pe = 1.03923 \neq 1$ in this case).

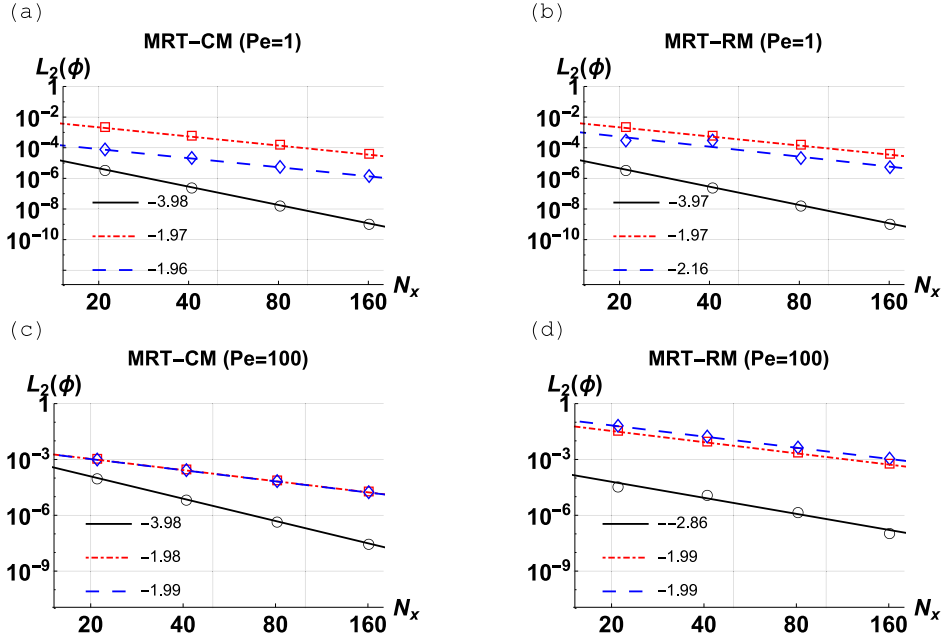


Fig. 12. Mesh convergence solutions of the time-decaying wave problem for $\bar{t} = 0.01$. Symbols: circles (black) use the free parameters $\{\omega_0, \Lambda_1, \Lambda\}$ that lead to $TE_3 = 0$ and $TE_4 = 0$, diamonds (blue) use $\omega_0 = 2/3$ and $\Lambda = 1/6$, and squares (red) use $\omega_0 = 2/3$ and $\Lambda = 1/12$. Insets quantify the converge rates given by the slopes of fitting lines obtained from linear regression. Panel (a): MRT-CM for $Pe = 1$ and $\epsilon = 0.1$. Panel (b): MRT-RM for $Pe = 1$ and $\epsilon = 0.1$. Panel (c): MRT-CM for $Pe = 100$ and $\epsilon = 0.01$. Panel (d): MRT-RM for $Pe = 100$ and $\epsilon = 0.01$.

The wave non-dimensional solution is $\bar{\phi} = \phi/\phi_0$. In this work, we consider the solution wavenumber $k_x = 2\pi$, the initial wave magnitude $\phi_0 = 1$ (simulation units), and the reference initial location $\bar{x}_0 = x_0/L = \frac{1}{2}$ (in non-dimensional units). The non-dimensional spatial domain coordinate is $\bar{x} = x/L \in [0, 1]$, with domain length L discretized as follows $L = N_x \Delta x$. Periodic boundary conditions are applied at both ends of the domain and the problem initial condition is given by Eq. (69) with $\bar{t} = 0$. Note that, for a given time evolution \bar{t} , the solution $\bar{\phi}$ is uniquely governed by Pe , which is set as follows $Pe = \frac{u/c}{\epsilon} N_x = \frac{u \Delta x N_x}{(1-\omega_0)c^2 \Lambda_1 \Delta t} = \frac{uL}{D}$. The other numerical parameters considered in this test are similar to those indicated before in Section 7.1.

Fig. 11 illustrates the LBM solutions, over the different collision operators, employing the free parameters $\{\omega_0, \Lambda_1, \Lambda\}$ that lead to the 4th order accurate solution, against the analytical profile, given by Eq. (69), for $Pe = 1$ and $\epsilon = 0.1$. The inability of the BGK collision operator to simultaneously fulfil the 4th order accurate condition and to exactly satisfy the intended Pe number is once again verified.

Fig. 12 depicts the evolution of the LBM numerical error for the MRT-CM and MRT-RM models at a given Pe as function of the N_x mesh resolution. The BGK model is not considered in this analysis for its inability to keep solutions parametrized by Pe as explained in Section 7.1. The numerical solutions in Fig. 12 share the trends displayed in Fig. 10 of Section 7.1. Both benchmark tests confirm the theoretical results presented in Section 5 in that the proper tuning of the free parameters $\{\omega_0, \Lambda_1, \Lambda\}$ that lead to $TE_3 = 0$ and $TE_4 = 0$ will recover 4th order accurate solutions; otherwise, the LBM solutions support a 2nd order accuracy. Numerical simulations appear to suggest that the MRT-CM model is less sensitive to the Pe number effect than the MRT-RM collision model. Yet, at the same time, the MRT-CM model is the more sensitive from a stability perspective, particularly when operating at larger advection velocities, as discussed in Section 6.1.

8. Conclusions

This paper performed a detailed theoretical analysis on the central moment (CM) space formulation of the LBM to model the 1D ADE, with a constant velocity and diffusion coefficient, based on the D1Q3 model. The research goal was threefold.

First, the discrete approximation of the CM-LBM towards the macroscopic ADE was clarified, without recurring to asymptotic analysis approaches, such as the Chapman–Enskog expansion. To this end, we derived the equivalent finite difference (EFD) scheme of the CM-LBM model. The developed consistency analysis allowed us to arrive at the following conclusions:

- In the D1Q3 setting, the CM-LBM satisfies an explicit four-level finite different (FLFD) scheme at discrete level, which is identical to the discrete structure of its raw moment (RM) space counterpart. The difference is that CM-LBM includes some extra velocity-dependent terms in the coefficients of the FLFD scheme.
- When the single-relaxation-time BGK collision is employed, these extra terms in CM-LBM formulation vanish. As a result, either CM or RM space formulations of the BGK scheme lead to exactly identical results (as they are governed by the exact same discrete schemes).
- The steady-state limit of this EFD scheme provides the modelled steady ADE of the considered LBM schemes. The CM-LBM recovers a steady ADE with an effective diffusion coefficient featuring an unphysical velocity dependency. This artefact can be made absent from the RM space formulation with a linear velocity equilibrium. Such a result discourages the use of the CM-LBM for steady-state ADE problems.

Second, the accuracy of the CM-LBM (and other collision models) with respect to the time-dependent ADE was investigated. To this end, we derived the equivalent partial differential (EPD) equations satisfied by these numerical schemes and examined the leading order truncation errors associated with each LBM collision model. The developed accuracy analysis provided the following conclusions:

- Among the studied models, the error structure of the CM-LBM displays the simpler and more compact form. This is particularly evident in the dispersion error term, which seems to justify the, often reported, improved Galilean invariance of the CM model.
- Through a suitable combination of the MRT free parameters, i.e. the weight coefficient and the two relaxation parameters, the CM-LBM accuracy can be improved from second- to fourth-order. The MRT-RM scheme also manages to improve its accuracy through this procedure. This contrasts with the REG and BGK collision models, which are unable to reach fourth-order accuracy by tuning its free parameters.

Third and final, the necessary and sufficient stability conditions of the CM-LBM, alongside with other collision models, were studied based on the von Neumann stability analysis of the EFD schemes previously derived. The stability analysis developed herein led to the following conclusions:

- Compared to the MRT-RM, the MRT-CM features extra terms that scale as u^6/c^6 , u^4/c^4 and u^2/c^2 . These terms may help stabilizing the solution, for $u/c \leq 0.5$, when the transport coefficient ϵ is small. However, for $u/c > 0.5$, they tend to dominate the overall stability condition, without a proper balance, causing the quick blow up of the solution (regardless the ϵ coefficient).
- Unlike the MRT-RM, the MRT-CM does not have an “optimal stability condition”, meaning it does not support a specific relaxation combination where its stability condition becomes unaffected by the individual relaxation rates values, and only controlled by the equilibrium parameters alone.

The aforementioned theoretical conclusions were all confirmed by numerical tests presented at the end of the manuscript. The benchmarks considered herein consisted of a Gaussian pulse and a sinusoidal wave, both cases defined over unbounded and infinite spatial domains. This way theoretical and numerical conclusions could be directly connected.

As next step in this study, we plan to extend the present work to 2D and 3D domains [60,62]. Nonetheless, as shown by Ginzburg and co-workers [45,71,73], the D1Q3 stability curves are able to provide reliable pictures (of the advection properties) of the multi-dimensional models, which underlines the value of the conclusion of the present study. Along the same lines, we also plan to extend this investigation to the approximation of other kinds of physical equations, such as the Navier–Stokes equations [59,60]. In this context, we note that for problems where the advection velocity is unknown, not only the analysis of the LBM-CM will become significantly more complex [59] but, more importantly, also its operation will become computationally more demanding due to the need to recompute the velocity matrix over each grid node at each time step. Hence, we foresee that future studies in this field should also focus on efficient ways to handle the LBM-CM implementation, where applications with the ADE are again a favourable starting point [74].

Declaration of competing interest

The author declares that he has no known competing financial interests or personal relationships that could have appeared to influence the work reported in this paper.

Acknowledgement

The author acknowledges Fundação para a Ciência e a Tecnologia (FCT) for its financial support via the project LAETA Base Funding (DOI: 10.54499/UIDB/50022/2020).

Data availability

Data will be made available on request.

References

- [1] Chen S, Doolen G. Lattice-Boltzmann method for fluid flows. *Annu Rev Fluid Mech* 1998;30:329. <http://dx.doi.org/10.1146/annurev.fluid.30.1.329>.
- [2] Aidun CK, Clausen JR. Lattice-Boltzmann method for complex flows. *Annu Rev Fluid Mech* 2010;42:439. <http://dx.doi.org/10.1146/annurev-fluid-121108-145519>.
- [3] Krüger T, Kusumaatmaja H, Kuzmin A, Shardt O, Silva G, Viggen EM. *The Lattice Boltzmann method - principles and practice*. first ed.. Springer; 2016, <http://dx.doi.org/10.1007/978-3-319-44649-3>.
- [4] Succi S. *The Lattice Boltzmann equation: for complex states of flowing matter*. Oxford University Press; 2018, <http://dx.doi.org/10.1093/oso/9780199592357.001.0001>.
- [5] Fletcher C. *Computational techniques for fluid dynamics 1*. second ed.. Berlin Heidelberg: Springer-Verlag; 1998, http://dx.doi.org/10.1007/978-3-642-58229-5_1.
- [6] Ferziger JH, Perić M, Street RL. *Computational methods for fluid dynamics*. fourth ed.. Springer; 2020, <http://dx.doi.org/10.1007/978-3-319-99693-6>.

- [7] Coreixas C, Chopard B, Latt J. Comprehensive comparison of collision models in the Lattice Boltzmann framework: Theoretical investigations. *Phys Rev E* 2019;100:033305. <http://dx.doi.org/10.1103/PhysRevE.100.033305>.
- [8] Qian YH, d'Humières D, Lallemand P. Lattice BGK models for Navier–Stokes equation. *Europhys Lett* 1992;17(6):479. <http://dx.doi.org/10.1209/0295-5075/17/6/001>.
- [9] Benzi R, Succi S, Vergassola M. The Lattice Boltzmann equation: Theory and applications. *Phys Rep* 1992;222:145. [http://dx.doi.org/10.1016/0370-1573\(92\)90090-M](http://dx.doi.org/10.1016/0370-1573(92)90090-M).
- [10] d'Humières D, Ginzburg I, Krafczyk M, Lallemand P, Luo LS. Multiple-relaxation-time Lattice Boltzmann models in three dimensions. *Philos Trans R Soc Lond Ser A* 2002;360:437. <http://dx.doi.org/10.1098/rsta.2001.0955>.
- [11] Geier M, Greiner A, Korvink JG. Cascaded digital Lattice Boltzmann automata for high Reynolds number flow. *Phys Rev E* 2006;73:066705. <http://dx.doi.org/10.1103/PhysRevE.73.066705>.
- [12] Dubois F, Février T, Graille B. Lattice Boltzmann schemes with relative velocities. *Commun Comput Phys* 2015;17:1088. <http://dx.doi.org/10.4208/cicp.2014.m394>.
- [13] Dubois F, Février T, Graille B. On the stability of a relative velocity Lattice Boltzmann scheme for compressible Navier–Stokes equations. *C R Méc* 2015;343:599. <http://dx.doi.org/10.1016/j.crme.2015.07.010>.
- [14] Fei L, Luo KH, Li Q. Consistent forcing scheme in the cascaded Lattice Boltzmann method. *Phys Rev E* 2017;96:053307. <http://dx.doi.org/10.1103/PhysRevE.96.053307>.
- [15] Fei L, Luo KH, Li Q. Three-dimensional cascaded Lattice Boltzmann method: Improved implementation and consistent forcing scheme. *Phys Rev E* 2018;97:053309. <http://dx.doi.org/10.1103/PhysRevE.97.053309>.
- [16] Rosis ADe, Luo KH. Role of higher-order Hermite polynomials in the central-moments-based Lattice Boltzmann framework. *Phys Rev E* 2019;99:013301. <http://dx.doi.org/10.1103/PhysRevE.99.013301>.
- [17] Wood LC. An introduction to the kinetic theory of gases and magnetoplasmas. Oxford: Oxford University Press; 1993. <http://dx.doi.org/10.1093/oso/9780198563938.001.0001>.
- [18] Premnath K, Banerjee S. On the three-dimensional central moment Lattice Boltzmann method. *J Stat Phys* 2011;143:747. <http://dx.doi.org/10.1007/s10955-011-0208-9>.
- [19] Lycett-Brown D, Luo KH. Multiphase cascaded Lattice Boltzmann method. *Comput Math Appl* 2014;67:350. <http://dx.doi.org/10.1016/j.camwa.2013.08.033>.
- [20] Shan X. Central-moment-based galilean-invariant multiple-relaxation-time collision model. *Phys Rev E* 2019;100:043308. <http://dx.doi.org/10.1103/PhysRevE.100.043308>.
- [21] Gruszczynski G, Laniewski-Woll L. A comparative study of 3D cumulant and central moments Lattice Boltzmann schemes with interpolated boundary conditions for the simulation of thermal flows in high Prandtl number regime. *Int J Heat Mass Transfer* 2022;197:123259. <http://dx.doi.org/10.1016/j.ijheatmasstransfer.2022.123259>.
- [22] Hajabdollahi F, Premnath KN. Symmetrized operator split schemes for force and source modeling in cascaded Lattice Boltzmann methods for flow and scalar transport. *Phys Rev E* 2018;97:063303. <http://dx.doi.org/10.1103/PhysRevE.97.063303>.
- [23] Sharma KV, Straka R, Tavares FV. New cascaded thermal Lattice Boltzmann method for simulations of advection-diffusion and convective heat transfer. *Int J Therm Sci* 2017;118:259–77. <http://dx.doi.org/10.1016/j.ijthermalsci.2017.04.020>.
- [24] Fei L, Luo KH. Cascaded Lattice Boltzmann method for thermal flows on standard Lattices. *Int J Therm Sci* 2018;132:368–77. <http://dx.doi.org/10.1016/j.ijthermalsci.2018.06.017>.
- [25] Straka R, Sharma KV. An accuracy analysis of the cascaded Lattice Boltzmann method for the 1D advection-diffusion equation. *Comput Methods Mater Sci* 2020;20(4):173–84. <http://dx.doi.org/10.7494/cmms.2020.4.0732>.
- [26] Hajabdollahi F, Premnath KN, Welch SWJ. Cascaded Lattice Boltzmann method based on central moments for axisymmetric thermal flows including swirling effects. *Int J Heat Mass Transfer* 2019;128:999–1016. <http://dx.doi.org/10.1016/j.ijheatmasstransfer.2018.09.059>.
- [27] Geier M, Greiner A, Korvink JG. A factorized central moment Lattice Boltzmann method. *Eur Phys J Spec Top* 2009;171:55. <http://dx.doi.org/10.1140/epjst/e2009-01011-1>.
- [28] Asinari P. Generalized local equilibrium in the cascaded Lattice Boltzmann method. *Phys Rev E* 2008;78:016701. <http://dx.doi.org/10.1103/PhysRevE.78.016701>.
- [29] De Rosis A. Non-orthogonal central moments relaxing to a discrete equilibrium: A D2q9 Lattice Boltzmann model. *Europhys Lett* 2016;116:44003. <http://dx.doi.org/10.1209/0295-5075/116/44003>.
- [30] De Rosis A. Nonorthogonal central-moments-based Lattice Boltzmann scheme in three dimensions. *Phys Rev E* 2017;95:013310. <http://dx.doi.org/10.1103/PhysRevE.95.013310>.
- [31] He X, Luo LS. Lattice Boltzmann model for the incompressible Navier–Stokes equation. *J Stat Phys* 1997;88:927. <http://dx.doi.org/10.1023/B:JOSS.00000015179.12689.e4>.
- [32] Siebert DN, Hegele Jr LA, Philippi PC. Lattice Boltzmann equation linear stability analysis: Thermal and athermal models. *Phys Rev E* 2018;77:026707. <http://dx.doi.org/10.1103/PhysRevE.95.013310>.
- [33] Wissocq G, Sagaut P. Hydrodynamic limits and numerical errors of isothermal Lattice Boltzmann schemes. *J Comput Phys* 2022;450:110858. <http://dx.doi.org/10.1016/j.jcp.2021.110858>.
- [34] Richtmyer RD, Morton KW. *Difference methods for initial-value problems*. New York: John Wiley & Sons; 1967.
- [35] Miller JJH. On the location of zeros of certain classes of polynomials with application to numerical analysis. *J Inst Math Appl* 1971;8:397–406. <http://dx.doi.org/10.1093/imamat/8.3.397>.
- [36] Warming RF, Hyett BJ. The modified equation approach to the stability and accuracy analysis of finite-difference methods. *J Comput Phys* 1974;14:159–79. [http://dx.doi.org/10.1016/0021-9991\(74\)90011-4](http://dx.doi.org/10.1016/0021-9991(74)90011-4).
- [37] Chapman S, Cowling TG. *The mathematical theory of nonuniform gases*. Cambridge: Cambridge University Press; 1970.
- [38] Junk M, Klar A, Luo L-S. Asymptotic analysis of the Lattice Boltzmann equation. *J Comput Phys* 2005;210:676. <http://dx.doi.org/10.1016/j.jcp.2005.05.003>.
- [39] Truesdell C, Muncaster RG. *Fundamentals of Maxwell's kinetic theory of a simple monatomic gas : treated as a branch of rational mechanics*. New York: Academic Press; 1980.
- [40] Yong W-A, Zhao W, Luo L-S. Theory of the Lattice Boltzmann method: Derivation of macroscopic equations via the Maxwell iteration. *Phys Rev E* 2016;93:033310. <http://dx.doi.org/10.1103/PhysRevE.93.033310>.
- [41] Holdych DJ, Noble DR, Georgiadis JG, Buckius RO. Truncation error analysis of Lattice Boltzmann methods. *J Comput Phys* 2004;193:595–619. <http://dx.doi.org/10.1016/j.jcp.2003.08.012>.
- [42] Wagner A. Thermodynamic consistency of liquid-gas Lattice Boltzmann simulations. *Phys Rev E* 2006;74:056703. <http://dx.doi.org/10.1103/PhysRevE.74.056703>.
- [43] Dubois F. Equivalent partial differential equations of a Lattice Boltzmann scheme. *Comput Math Appl* 2008;55:1441. <http://dx.doi.org/10.1016/j.camwa.2007.08.003>.
- [44] d'Humières D, Ginzburg I. Viscosity independent numerical errors for Lattice Boltzmann models: from recurrence equations to magic collision numbers. *Comp Math Appl* 2009;58(5):823–40. <http://dx.doi.org/10.1016/j.camwa.2009.02.008>.
- [45] Ginzburg I. Truncation errors, exact and heuristic stability analysis of two-relaxation-times Lattice Boltzmann schemes for anisotropic advection-diffusion equation. *Commun Comput Phys* 2012;11:1439. <http://dx.doi.org/10.4208/cicp.211210.280611a>.
- [46] Chai Z, Shi B. Multiple-relaxation-time Lattice Boltzmann method for the Navier–Stokes and nonlinear convection diffusion equations: Modeling, analysis, and elements. *Phys Rev E* 2020;102:023306. <http://dx.doi.org/10.1103/PhysRevE.102.023306>.
- [47] Silva G, Semiao V. Truncation errors and the rotational invariance of three-dimensional Lattice models in the Lattice Boltzmann method. *J Comput Phys* 2014;269:259–79. <http://dx.doi.org/10.1016/j.jcp.2014.03.027>.
- [48] Guo Z, Zheng C, Shi B. Force imbalance in Lattice Boltzmann equation for two-phase flows. *Phys Rev E* 2011;83:036707. <http://dx.doi.org/10.1103/PhysRevE.83.036707>.
- [49] Silva G. Discrete effects on the forcing term for the Lattice Boltzmann modeling of steady hydrodynamics. *Comput Fluids* 2020;203:104537. <http://dx.doi.org/10.1016/j.compfluid.2020.104537>.
- [50] He X, Zou Q, Luo L-S, Dembo M. Analytical solutions of simple flows and analysis of nonslip boundary conditions for the Lattice Boltzmann BGK model. *J Stat Phys* 1997;87:115–36. <http://dx.doi.org/10.1007/BF02181482>.
- [51] Ginzburg I, Silva G, Talon L. Analysis and improvement of Brinkman Lattice Boltzmann schemes: Bulk, boundary, interface. Similarity and distinctness with finite elements in heterogeneous porous media. *Phys Rev E* 2015;91:023307. <http://dx.doi.org/10.1103/PhysRevE.91.023307>.
- [52] Cui S, Hong N, Shi B, Chai Z. Discrete effect on the halfway bounce-back boundary condition of multiple-relaxation-time Lattice Boltzmann model for convection–diffusion equations. *Phys Rev E* 2016;93:043311.
- [53] Ancona MG. Fully Lagrangian and Lattice-Boltzmann methods for solving systems of conservation equations. *J Comput Phys* 1994;155:107–20. <http://dx.doi.org/10.1006/jcph.1994.1181>.
- [54] Suga S. An accurate multi-level finite difference scheme for 1D diffusion equations derived from the Lattice Boltzmann method. *J Stat Phys* 2010;140:494–503. <http://dx.doi.org/10.1007/s10955-010-0004-y>.

- [55] Succi S. A note on the Lattice Boltzmann versus finite-difference methods for the numerical solution of the Fisher's equation. *Int J Mod Phys C* 2014;25:1340015. <http://dx.doi.org/10.1142/S0129183113400159>.
- [56] Dellacherie S. Construction and analysis of Lattice Boltzmann methods applied to a 1D convection-diffusion equation. *Acta Appl Math* 2014;131:69. <http://dx.doi.org/10.1007/s10440-013-9850-3>.
- [57] Lin Y, Hong N, Shi B, Chai Z. Multiple-relaxation-time Lattice Boltzmann model-based four-level finite-difference scheme for one-dimensional diffusion equations. *Phys Rev E* 2021;104:015312. <http://dx.doi.org/10.1103/PhysRevE.104.015312>.
- [58] Silva G. Discrete effects on the source term for the Lattice Boltzmann modelling of one-dimensional reaction–diffusion equations. *Comput Fluids* 2021;251:105735. <http://dx.doi.org/10.1016/j.compfluid.2022.105735>.
- [59] Fúciók R, Straka R. Equivalent finite difference and partial differential equations for the Lattice Boltzmann method. *Comput Math Appl* 2021;90:96–103. <http://dx.doi.org/10.1016/j.camwa.2021.03.014>.
- [60] Bellotti T, Graïlle B, Massot M. Finite difference formulation of any Lattice Boltzmann scheme. *Numer Math* 2022;152:1. <http://dx.doi.org/10.1007/s00211-022-01302-2>.
- [61] Chen Y, Chai Z, Shi B. Fourth-order multiple-relaxation-time Lattice Boltzmann model and equivalent finite-difference scheme for one-dimensional convection–diffusion equations. *Phys Rev E* 2023;107:055305. <http://dx.doi.org/10.1103/PhysRevE.107.055305>.
- [62] Chen Y, Chai Z, Shi B. A general fourth-order mesoscopic multiple-relaxation-time Lattice Boltzmann model and its macroscopic finite-difference scheme for two-dimensional diffusion equations. *J Comput Phys* 2024;509:113045. <http://dx.doi.org/10.1016/j.jcp.2024.113045>.
- [63] Chen Y, Liu X, Chai Z, Shi B. Macroscopic finite-difference scheme and modified equations of the general propagation multiple-relaxation-time Lattice Boltzmann model. *Phys Rev E* 2024;109:065305. <http://dx.doi.org/10.1103/PhysRevE.109.065305>.
- [64] Bennett T. *Transport by advection and diffusion*. first ed.. Wiley; 2012.
- [65] Yoshida H, Nagaoka M. Multiple-relaxation-time Lattice Boltzmann model for the convection and anisotropic diffusion equation. *J Comput Phys* 2010;229:7774. <http://dx.doi.org/10.1016/j.jcp.2010.06.037>.
- [66] Ginzburg I. Multiple anisotropic collisions for advection diffusion Lattice Boltzmann schemes. *Adv Water Resour* 2013;51:381. <http://dx.doi.org/10.1016/j.advwatres.2012.04.013>.
- [67] Karlin IV, Lycett-Brown D, Luo KH. Enhanced Lattice bhatnagar-gross-krook method for fluid dynamics simulation. 2011, doi:10.48550/arXiv.1107.3309.
- [68] Ginzburg I. Equilibrium-type and link-type Lattice Boltzmann models for generic advection and anisotropic-dispersion equation. *Adv Water Resour* 2005;28:1171–95. <http://dx.doi.org/10.1016/j.advwatres.2005.03.004>.
- [69] Chopard B, Falcone JL, Latt J. The Lattice Boltzmann advection-diffusion model revisited. *Eur Phys J Spec Top* 2009;171:245–9. <http://dx.doi.org/10.1140/epjst/e2009-01035-5>.
- [70] Ginzburg I, Silva G, Marson F, Chopard B, Latt J. Unified directional parabolic-accurate Lattice Boltzmann boundary schemes for grid-rotated narrow gaps and curved walls in creeping and inertial fluid flows. *Phys Rev E* 2023;107:025303. <http://dx.doi.org/10.1103/PhysRevE.107.025303>.
- [71] Kuzmin A, Ginzburg I, Mohamad AA. A role of the kinetic parameter on the stability of two-relaxation-times advection-diffusion Lattice Boltzmann scheme. *Comp Math Appl* 2011;61:3417–42. <http://dx.doi.org/10.1016/j.camwa.2010.07.036>.
- [72] Chikatamarla SS, Karlin IV. Lattices for the Lattice Boltzmann method. *Phys Rev E* 2009;79:046701. <http://dx.doi.org/10.1103/PhysRevE.79.046701>.
- [73] Ginzburg I, d'Humières D, Kuzmin A. Optimal stability of advection-diffusion Lattice Boltzmann models with two relaxation times for positive/negative equilibrium. *J Stat Phys* 2010;139(6):1090–143. <http://dx.doi.org/10.1007/s10955-010-9969-9>.
- [74] Wawrzyniak D, Winter J, Schmidt S, Indinger T, Janßen CF, Schramm U, Adams NA. A quantum algorithm for the Lattice-Boltzmann method advection-diffusion equation. *Comput Phys Comm* 2025;306:109373. <http://dx.doi.org/10.1016/j.cpc.2024.109373>.